Analyst

TUTORIAL REVIEW

View Article Online
View Journal | View Issue

Cite this: *Analyst*, 2023, **148**, 2901

Sum frequency generation spectroscopy of fluorinated organic material-based interfaces: a tutorial review

Siwakorn Sakunkaewkasem,[a,b] Daniela Deleon,[a] Yunsoo Choi,[a] Hung-Vu Tran,[a] Maria D. Marquez,[a] Steven Baldelli*[a] and T. Randall Lee*[a]

Received 11th December 2022,
Accepted 6th May 2023

DOI: 10.1039/d2an02020c

rsc.li/analyst

Molecular interactions at interfaces have a significant effect on the wetting properties of surfaces on a macroscale. Sum frequency generation (SFG) spectroscopy, one of a few techniques capable of probing such interactions, generates a surface vibrational spectrum sensitive to molecular structures and has been used to determine the orientation of molecules at interfaces. The purpose of this review is to assess SFG spectroscopy's ability to determine the molecular orientations of interfaces composed of fluorinated organic molecules. We will explore three different types of fluorinated organic material-based interfaces, naming liquid–air, solid–air, and solid–liquid interfaces, to see how SFG spectroscopy can be used to gain valuable and unique information regarding the molecular orientation of each interface. We hope this review will help to broaden the understanding of how to employ SFG spectroscopy to obtain more complex structural information for various fluorinated organic material-based interfaces in the future.

1. Introduction

The interface between two media, where molecules are exposed to an environment different from that found in the bulk, is where the chemical interactions (*i.e.*, van der Waals interactions and hydrogen bonds) take place and dictates how the two media behave macroscopically. For example, it is well established that hydrophobic materials, such as polytetrafluoroethylene (PTFE), exhibit a low surface wettability, allowing water drops to easily roll off these surfaces due to the poor chemical interactions between the atoms on their surfaces and water molecules.[1–3] These phenomena can only be explained by meticulously examining atoms and molecules at buried interfaces to ascertain their composition, structure conformation, orientation, and bond interactions between two media. Among these interfaces, solid–liquid and solid–air interfaces can provide extremely valuable information about the orientation of contact liquids, the orientation of terminal groups on surfaces, and molecular interactions that affect the macroscale properties of a surface.[4–7] Numerous surface analytical techniques including ellipsometry, contact angle goniometry, Raman spectroscopy, X-ray photoelectron spectroscopy (XPS), and infrared spectroscopy, such as polarization modulation-infrared reflection-adsorption spectroscopy (PM-IRRAS)[6,8] have been used to investigate properties of various organic-based surfaces, such as their basic structural orientations, wettability, and chemical compositions at interfaces.[4,5,9] Additionally, atomic force microscopy (AFM) has also been utilized to obtain detailed information about the nanometric lateral resolution of such surfaces.[10–12] This technique, however, is limited in its ability to provide an advanced understanding of buried surfaces, such as the direction and interaction of different types of liquids in contact with solid interfaces, or the tilt angle and conformational features at solid–air and solid–liquid interfaces. Interestingly, while all of the aforementioned techniques provide valuable data that broaden our understanding of surface and interfacial chemistry at nanoscales, valuable insight into buried surfaces can be obtained only from a unique surface-sensitive technique called sum-frequency generation vibrational spectroscopy (SFG-VS).[4,13,14] A quick summary and comparison between SFG and other surface techniques are illustrated in Fig. 1.

SFG-VS is a coherent second-order nonlinear optical spectroscopy technique that is used to analyze interfaces and surfaces. In a typical SFG-VS, two optical sources combine at the probed interface to generate an output beam with a frequency equal to the sum of the visible and infrared photons, as illustrated in Fig. 2.[14] Due to the SFG signal generated by each

[a]*Department of Chemistry and the Texas Center for Superconductivity, University of Houston, 4800 Calhoun Road, Houston, TX 77204-5003, USA. E-mail: sbaldelli@uh.edu, trlee@uh.edu*
[b]*Solar Photovoltaic Research Team, National Energy Technology Center, National Science and Technology Development Agency, 114 Thailand Science Park, Phaholyothin Road, Klong Nueng, Klong Luang, Pathum Thani 12120, Thailand*

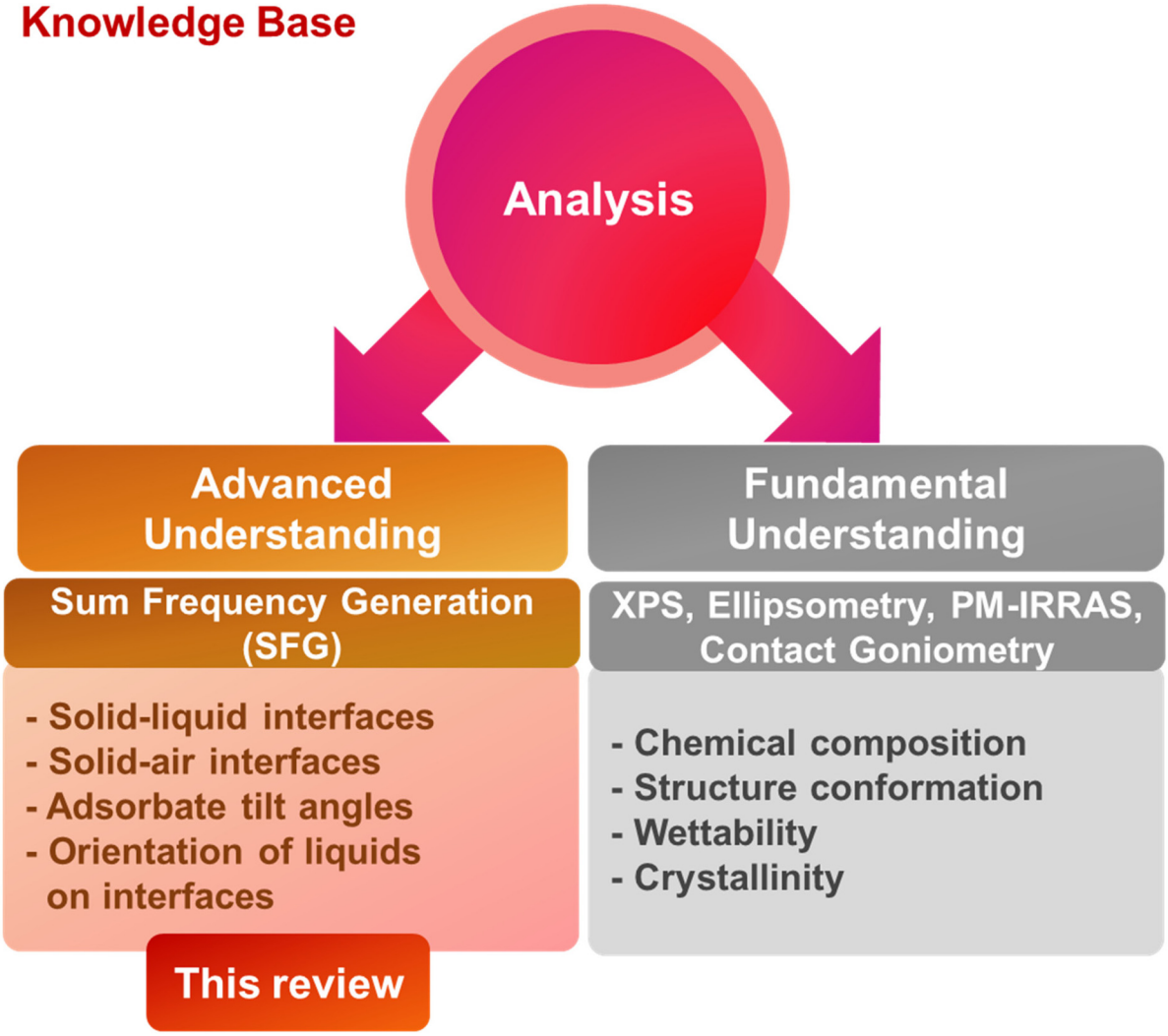

Fig. 1 Advanced surface information of organic thin films probed with SFG technique compared to other surface techniques.

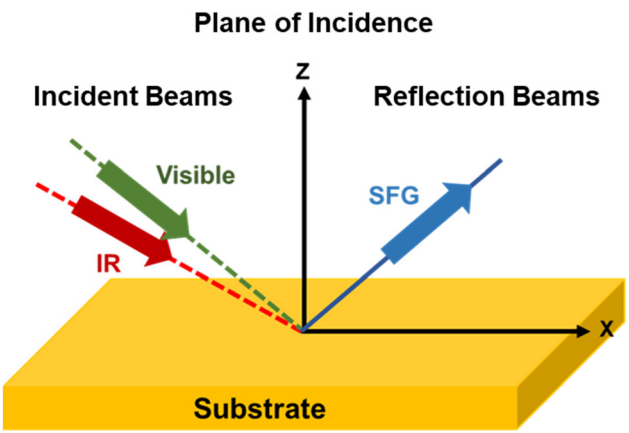

Fig. 2 Illustration of two laser beams, a visible beam (green arrow) and an infrared beam (red arrow), incident on a substrate from which the sum frequency generation (SFG) laser beam is generated. The illustration is not to scale, and the area covered by the laser beams is on the order of one millimeter.

measurement is quite weak, despite the fact that SFG equipment is normally equipped with extremely bright visible and infrared sources, the obtained signal is still quite low. However, the output signal generated by the SFG technique is free of background signal due to the nonlinear mixing process. The intensity output from SFG is estimated by fitting the resonances to a Lorentzian line shape according to eqn (1),[15–18] where I_{SFG} is the intensity of the SFG signal, $\chi_R^{(2)}$ and $\chi_{NR}^{(2)}$ are the resonant and nonresonant contributions to the second-order nonlinear susceptibility, A_q and Γ_q denote the amplitude and linewidth of the qth vibrational mode at a frequency of ω_q, the infrared frequency is ω_{IR}, A_{NR} and ε are the nonresonant amplitude and phase of the substrate, respectively.

$$I_{SFG} \propto \left|\chi_R^{(2)} + \chi_{NR}^{(2)}\right|^2 = \left|\sum_q \frac{A_q}{\omega_q - \omega_{IR} - i\Gamma_q} + A_{NR}e^{i\varepsilon}\right|^2 \quad (1)$$

By selecting different polarization combinations of the input and output light (typically ssp, ppp, sps, and pss where

the indexes refer to the SF, visible, and IR beams, respectively), the Cartesian components of the susceptibility tensor $\chi^{(2)}$ can be deduced. Since the magnitude of the measured susceptibility tensor is sensitive to the degree of the polar orientation of the molecules, the information provided by the polarization analysis of the interface allows a determination of the molecular orientation with respect to the surface normal.[19]

The primary advantage of the SFG-VS technique is its ability to probe the vibrational frequencies/modes and electronic properties of the surface when the initial frequencies from the infrared and visible sources are tuned properly.[20,21] Additionally, chemically specific information such as molecular number density, molecular conformations and orientations, chemical change dynamics, and relaxations of molecular surfaces and interfaces can also be obtained.[14] More detailed explanation of the SFG technique are available in the literature.[15,22,23]

The fabrication of "tunable interfaces", whose physical, chemical, or electronic properties can be dynamically modified or tuned, can be accomplished by applying external stimuli such as temperature, pressure, electric or magnetic fields, or by altering the interfacial composition or morphology. Deposition of organic thin films on metal substrates *via* self-assembled monolayers (SAMs) has been reported and widely used to develop monolayer organic thin films on such interfaces, as well as to control the properties of metal surfaces at the nanoscale.[24–29] Numerous solid–liquid and solid–air interfaces have been investigated using these model surfaces composed of self-assembled and chemically bound molecules on a surface due to the monolayers' ability to mimic the physical properties of more complex systems.[5,30–33] These monolayer thin films have been used in a wide variety of applications, including biologically relevant surfaces,[34–38] lubricants for microelectromechanical systems (MEMs),[39–41] and corrosion inhibitors.[42–47]

Notably, the physical properties of organic thin films can be altered by the type of functional groups on the adsorbate molecules. For example, SAMs generated from *n*-alkanethiols with a chain length greater than 10 carbons exhibit a trans-extended configuration, tilted ~30° from the surface normal on Au substrates due to the presence of attractive van der Waals forces between the adjacent alkyl chains.[30,48–51] Investigation of the interfacial structure of alkanethiol thin films revealed significant implications for their wetting properties.[41,52,53] Specifically, altering the length of the alkanethiol adsorbates by changing the number of carbon atoms in the alkyl chain results in an alteration of the terminal functional groups' orientation (upright or tilted). This change in terminal group orientation has been shown to originate "odd–even" effect in the wettability of the surfaces and can be observed by advancing contact angle measurements.[52–59]

Changing the terminal functional group of a monolayer to a group other than the *n*-alkyl moiety has been shown to have a direct effect on the resulting film's physical properties.[52,60–68] It has been demonstrated that using terminal fluorinated tailgroups has a significant effect on the interfacial properties of the thin films in unexpected ways.[4,31,54,69] Due to the increased steric constraints and the helix-like structure of the fluorinated tailgroups, the tilt angles of fluorinated organic thin films relative to the surface normal were found to be significantly smaller than that of *n*-alkanethiol-based SAMs. Moreover, because of the low surface energies of fluorinated groups,[70] fluorinated SAMs exhibit remarkably lower wettabilities than organic thin films generated from *n*-alkanethiols.[54] Additionally, the surface dipole effect generated by the CF–CH junction has a crucial effect on the wettability of SAM surfaces; specifically, the dipole of the terminal CF–CH bond has a strong influence on the "odd–even" effect, as indicated by the inverse "odd–even" trend observed for polar aprotic liquids.[54,71] This phenomenon was rationalized based on compensation between the adjacent dipoles and the contacting liquid, which leads to diminished dipole–dipole interactions with contacting liquids for thin films with more titled chains than for thin films with more upright chains. This behavior is in contrast to normal SAMs (*e.g.*, *n*-alkanethiol-based SAMs) with markedly weaker surface dipoles exposed at their interfaces.[54,71] However, the dipole effect can be intentionally reduced by increasing the degree of fluorination, which corresponds to dipoles being buried deeper into the monolayer. Consequently, a significant decrease in film wettability was recorded when the number of terminal fluorinated carbon atoms on the chain of the absorbate molecule increased.[54,71]

Understanding fundamental interfacial properties (*e.g.*, conformation, dipole moment change, and interfacial structure) of fluorinated SAMs and other fluorinated organic material-based interfaces enables the development of new types of organic thin films and organic material-based interfaces with precise control over desired interfacial properties. In consideration of that, this review highlights key studies that employed SFG technique to investigate fluorinated-based organic thin films and fluorinated organic material-based interfaces in order to gain a better understanding of these unique types of interfaces with a focus on liquid–air, solid–liquid, and solid–air interfaces. Table 1 provides an overview of data types and key information obtained from SFG technique for each category.

2. SFG spectroscopy to probe fluorinated material-based liquid–air interfaces

Finding molecular dynamics and interactions at the air–liquid interfaces of fluorinated molecules are of paramount interest due to their potential applications in industry and medicine, as well as providing valuable and fundamental understandings of surface and interface chemistry at nanoscales.[72–74] The simplest molecular structure of semifluorinated compounds that form monolayers at air/water interfaces can be presented in a general formula of $CF_3(CF_2)_m(CH_2)_nH$.[75,76] Moreover, semi-fluorinated amphiphiles, which embed a polar group (*e.g.*,

Table 1 Data types and key information obtained from SFG spectroscopy for liquid–air, solid–air, and solid–liquid fluorinated organic material-based interfaces

Types of interfaces	Data obtained from SFG	Key information
Liquid–air interfaces	- Molecular arrangements	- Explore molecular orientations and conformations and/or disordered surface structures of fluorinated groups at liquid/air interfaces
Solid–air interfaces	- Molecular arrangements	- Depict proposed molecular arrangement of fluorinated groups in films with centrosymmetric and one-direction headgroup ordering
	-Extraordinary interfacial properties	- Rationalize the extraordinary advancing contact angle patterns where fluorinated groups act as a surrogate surface
Solid–liquid interfaces	- Liquid orientations on interfaces	- Confirm alignment of liquid interactions based on the directions of the dipole moment of surface fluorinated functional groups

alcohol, carboxylic acid, and thiol) into a non-polar fluorinated hydrocarbon chain, enhance the stability of molecules at air–water interfaces *via* forming monolayers, bilayers, and micelles.[74,77] For characterizing these interfaces, routine surface techniques, such as X-ray, atom scattering spectroscopy, infrared adsorption and Raman scattering spectroscopies, are not appropriate to use for air–liquid systems due to the probing interfaces requiring stability under a high vacuum environment, while the optical techniques ranging from infrared spectroscopy to ellipsometry are not surface-specific because the obtained signals from these methods are governed dominantly by molecules in the material bulk; the bulk contains a larger amount of molecules compared to the relatively small number of molecules at the outer layers of the surfaces.[78,79] On the other hand, SFG spectroscopy, a nonlinear optical technique, is a powerful technique for studying the dynamics of molecules at air–liquid interfaces due to its surface-specific properties, producing signals only at surfaces where the inversion symmetry of molecules is destroyed. Thus, SFG output generates a spectrum of the air–liquid interfaces and provides meaningful information about molecular orientation, conformation, as well as structure of the surface. Consequently, SFG spectroscopy has come into use for fluorinated molecules in the C–F stretching region at various air–liquid interfaces, even though such studies showed difficulties in the accurate assignment of the resonances in the spectra and the determination of CF_3 group orientations at the interfaces in some cases.[77,80–82]

In 2007, Tyrode *et al*. used SFG spectroscopy to study the air–water interface of a monolayer generated *via* ammonium perfluorononanoate (**APFN**) (Fig. 3a).[80] In this study, SFG spectra of the CF_3 and COO^- stretching allowed an estimation of the orientations of the headgroup and tailgroup of **APFN**. The SFG spectra at the critical micellar concentration of **APFN** (8.9 mM) exhibited two distinct overlapping peaks at 1369 and 1408 cm^{-1} under the ssp and ppp polarization combinations. In the meanwhile, the sps spectrum showed the strongest peak at 1665 cm^{-1} as shown in Fig. 3b. The peak at 1408 cm^{-1} was assigned to the symmetric carboxylate stretch ($\nu_s^{COO^-}$) based on previous bulk IR and Raman studies while the peak at 1665 cm^{-1} in the sps spectrum was determined as the antisymmetric stretch of the carboxylate group ($\nu_a^{COO^-}$). Unfortunately, the determination of peaks ranging from 1320–1380 cm^{-1} was ambiguous, but they had a relationship with the fluorocarbon vibrations, contributing either to axial symmetric CF_2 stretching vibration or to the vibration of the terminal CF_3 group. To support the peak assignments in the CF region, the authors provided additional SFG spectra of a monolayer of 2,2,3,3,4,4,5,5,6,6,7,7,8,8,9,9-hexadecafluorononanoic acid (**F16C9** acid), which possesses a terminal CF_2H instead of CF_3 group (Fig. 3a). The ssp and ppp spectra of the air–water interface of **F17C9** acid monolayers at 1369 cm^{-1}, which was also observed in the **APFN** monolayers, exhibited the plausible asymmetric CF_3 stretch. On the other hand, the absence of the peak at 1369 cm^{-1} in the SFG spectra of the CF_2H-terminated **F16C9** acid monolayer under the ssp and ppp polarization combinations provided strong evidence of the asymmetric CF_3 vibration at 1369 cm^{-1} while the axial CF_2 stretch was still observed in these spectra (Fig. 3c and d). Based on the assigned frequency of the CF_2/CF_3 and COO^- stretching vibrations, the authors showed that SFG is a powerful tool to analyze the orientations of fluorinated surfactants at air–water interfaces. The results showed that the COO^- and the CF_3 group showed slightly and significantly tilted angles from the surface normal (30–40° and 60–70°), respectively. Moreover, while the average orientations of terminal CF_3 and carboxylate groups remain constant at air–liquid surfaces at concentrations above 1 mM with no evidence of *gauche* defects in the fluorocarbon chain, an increase in the tilt angles of both groups makes them more lying to the surface plane at concentrations below 1 mM.

In 2008, Iwahashi *et al.* examined the structure and configuration of the triflate anion ($^-$Otf) at the air/1-butyl-3methylimidazolium trifluoromethansulfonate ([bmim]OTf) interface using SFG spectroscopy (Fig. 4a).[81] The SFG spectra of [bmim]OTf under ssp and ppp polarizations in Fig. 4c showed two distinct peaks. The peaks at 1043 and 1231 cm^{-1} were assigned to the symmetric stretch of SO_3^- and CF_3 groups, respectively, while the strong peak at ~1162 cm^{-1} in the IR spectra of [bmim]OTf showed in Fig. 4b is not prominent in the SFG spectra because of the weak Raman activity. For the SFG spectrum of LiOTf(aq) shown in Fig. 4e, the peaks at 1059 and 1237 cm^{-1} correspond to the symmetric stretch of SO_3^- and CF_3, respectively. Notably, the SFG spectra shown in Fig. 4c and d exhibited the opposite asymmetric shapes of the sym-

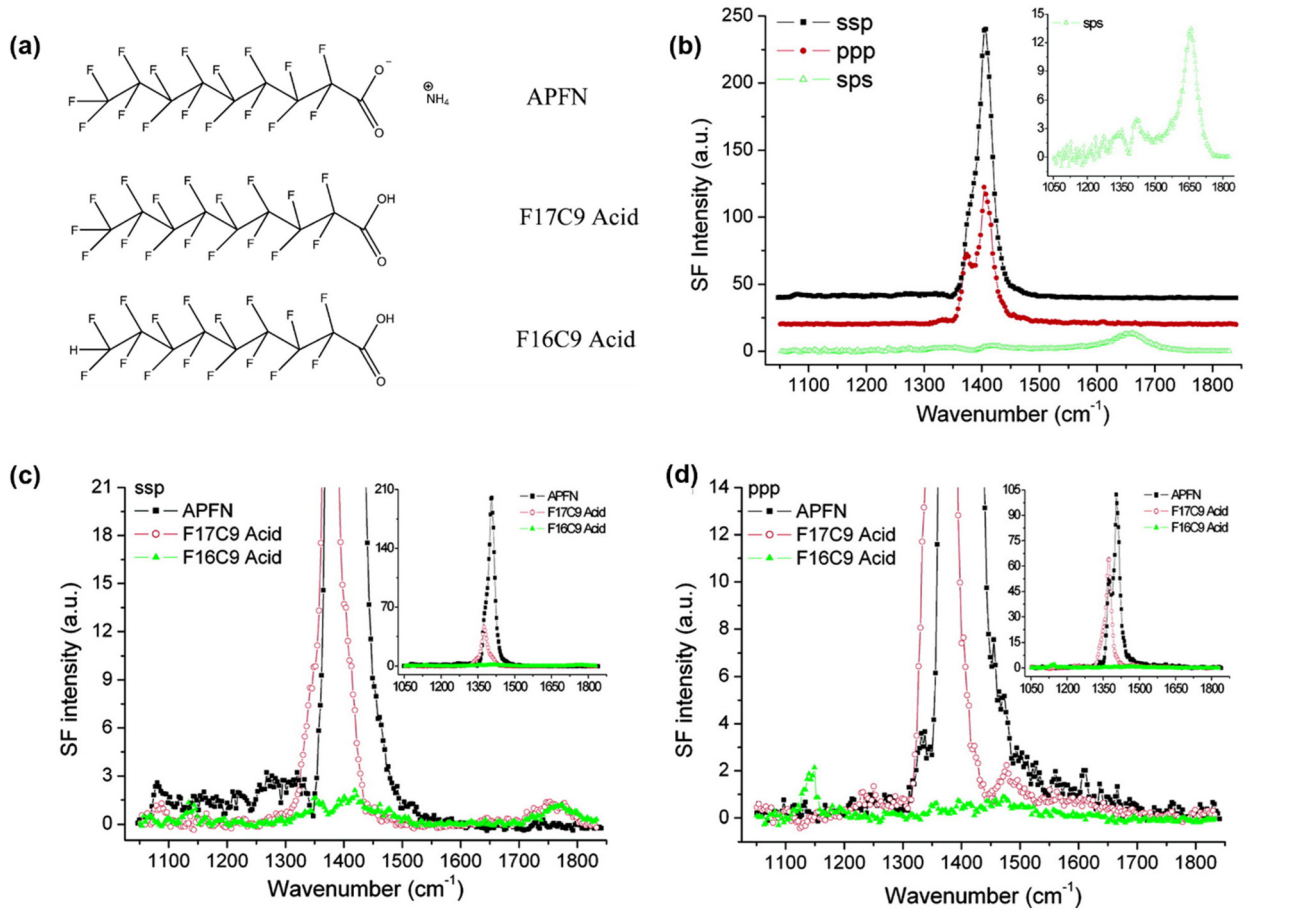

Fig. 3 (a) Molecular structures of the **APFN**, **F17C9** acid, and **F16C9** acid. (b) SFG spectra for **APFN** solution at 11.6 mM obtained under the ssp, ppp, and sps polarization combinations. SFG spectra for **APFN**, **F17C9** acid, and **F16C9** acid solutions under the ssp (c) and ppp (d) polarization combinations. Reproduced from ref. 80 with permission from [American Chemical Society], copyright [2007].

metric SO_3^- and CF_3 stretches, and *ab initio* calculations indicated that the orientation of the CF_3 group of $^-$OTf anion points away from the bulk liquid while the SO_3^- group points toward the bulk liquid. Furthermore, by comparing SFG spectra with the bulk IR (Fig. 4b and c), the structural difference of [bmim]OTf at the surface and in the bulk was able to be evaluated. The peak positions of the symmetric stretch of CF_3 at ~1231 cm^{-1} were similar in both the IR and SF spectra, implying that the SO_3^- group interacts strongly with the $[bmim]^+$ cations. The peak position at 1043 cm^{-1} of the symmetric stretch of SO_3^- in the SP spectra shown in Fig. 4c was blue-shifted by ~12 cm^{-1} and had a much sharper peak compared to that in the bulk IR shown in Fig. 4b, indicating that the $^-$OTf anion had better homogeneously and strongly interactions with the neighboring molecule $[bmim]^+$ cations at the surface than in the bulk. Moreover, the broad bulk IR peak at 1032 cm^{-1} in Fig. 4b reversely showed that the $^-$OTf anions of [bmim]OTf loosely interacted with $[bmim]^+$ cations in the bulk.

Karageorgiev *et al.* analyzed the average conformations of docosyl ethyl ether (EE) and docosyl trifluoroethyl ether (FEE) monolayers at air/water interfaces despite the limitations of classical SFG spectroscopy where the SFG signal is proportional to the square of the interfacial nonlinear susceptibility and does not yield the net polar orientation of interfacial water.[82] Instead, to determine the rearrangement of the neat water surface caused by the FEE headgroup, the author restricts the analysis to the peak of the free OH groups whose positive polar orientation is well-known.[82] Normally, monolayers formed from nonfluorinated amphiphiles create a positive dipole potential at the boundary with water while monolayers with CF_3 terminal polar headgroups (*e.g.*, OCH_2CF_3) generate a negative dipole: monolayers, bilayers, micelles, or biomembranes generated from natural nonionic amphiphiles orient the positive sign of the polar moiety toward the nonpolar group, forming a positive dipole potential at the air/water boundary. To determine the conformation of the polar heads of monolayers, the authors used a three-capacitor model by applying eqn (2):

$$\Delta V = \left(\frac{\mu_{w,\perp}}{\varepsilon_w} + \frac{\mu_{h,\perp}}{\varepsilon_h} + \frac{\mu_{t,\perp}}{\varepsilon_t}\right)/\varepsilon_0 A \qquad (2)$$

here ΔV is the surface potential of the monolayer, A is the area per amphiphilic molecule, ε is the effective dielectric permittivity of the film and μ is the molecular dipole moment

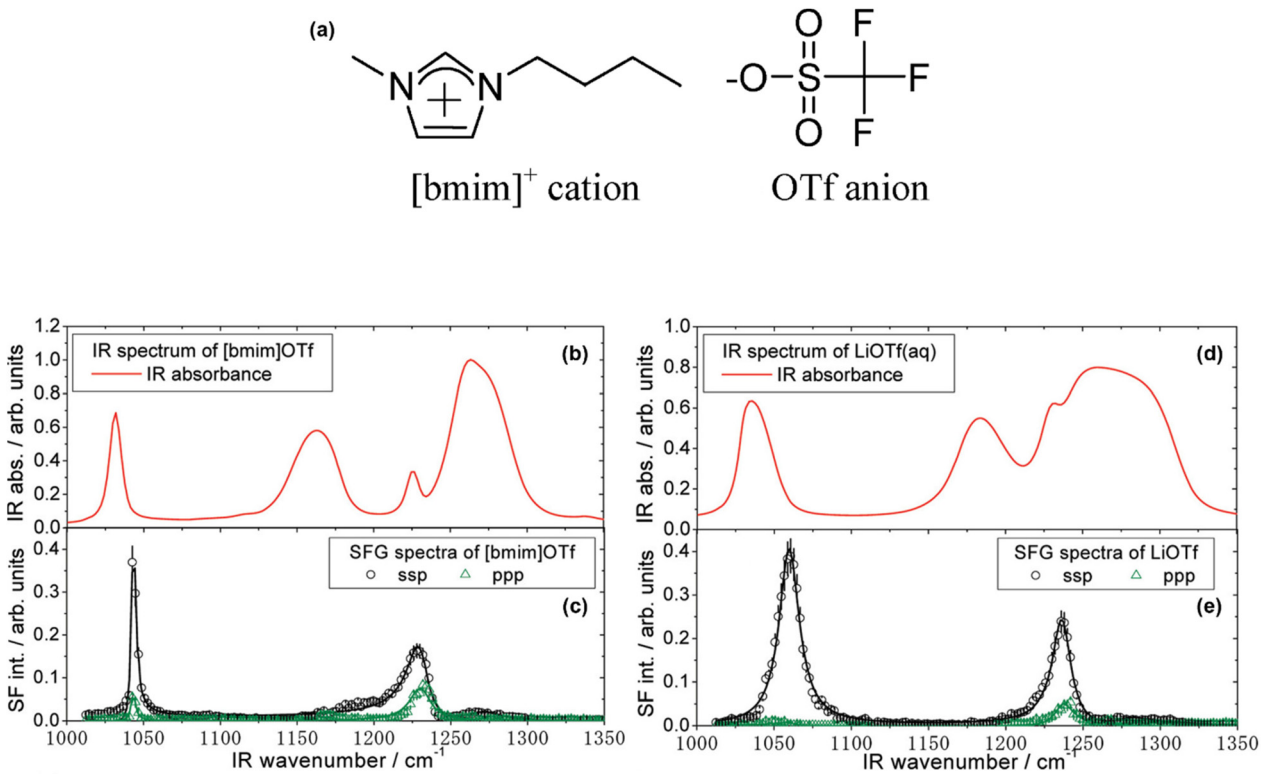

Fig. 4 (a) Structures of the ionic liquid, (b and d) IR spectra of [bmim]OTf and LiOTf, (c and e) SFG spectra of [bmim]OTf and LiOTf under the ssp and ppp polarization combinations. Reproduced from ref. 81 with permission from [American Chemical Society], copyright [2008].

(w: from the rearrangement of the interfacial water dipoles by the monolayer, h: from the dipoles of the hydrophilic head, and t: from the CH_3 terminals of the hydrocarbon tails). In Fig. 5a, the 3200 cm^{-1} peak of the pure water surface was blue-shifted by 100 cm^{-1} in the spectra of EE hydration water along with the decrease of peak intensity below the 3350 cm^{-1} region. The extinct discrepancy between the ssp spectra of neat water and the ssp spectra of EE hydration water exhibited a rearrangement from the pure water surface, which stemmed from a strong short-range interaction between the polar headgroups of EE (OCH_2CH_3) and water. On the other hand, the spectrum of the FEE hydration water is accordant with the spectrum of the neat water surface at the region below 3600 cm^{-1} as shown in Fig. 5b. It means that the headgroups of FEE (OCH_2CF_3) would be unable to disrupt the coordinated system of water. The increase of oscillator strength of the free OH is, however, the positive $\frac{\mu_{w,\perp}}{\varepsilon_w}$ term that cannot be responsible for the negative potential of the FEE monolayer. One possible contributor to the negative potential of FEE monolayer is that the polar headgroup on FEE monolayer predominates to the *trans–trans–gauche* conformation (upward oriented C–F bond in Fig. 5c – right confirmation) so that such negative dipole moment component of the C–F bond on the upward polar headgroup contributed to the negative dipole potential of the FEE monolayer while the same orientation of EE headgroups contributed to the positive term.

Most recently, Volpati *et al.* expanded the study of fluorinated alkane molecules at air–water surfaces to elucidate the influence of the length of the fluorinated- or hydrogenated segments.[77] In the study, a series of Langmuir monolayers of semifluorinated thiols $\mathbf{C_mF_{2m+1}C_nH_{2n}SH}$ were characterized by SFG spectroscopy, leading to a better understanding of the orientation and structure of the semi-fluorinated chains in surfaces of these monolayers. The peak assignments for semi-fluorinated thiol **F10H10SH** Langmuir monolayer was demonstrated by comparing its SFG spectrum with spectra of semi-flourinated carboxylic acid **F10H10COOH** and alcohol **F10H10OH** monolayers. The summarized values obtained under the ssp and sps polarization combinations are summarized in Table 2. Moreover, the peak intensities for CH_2-ss^G at 2845 cm^{-1}, which was arising from a *gauche* defect in the chain, and CH_2-ss^P at 2874 cm^{-1}, which symmetric methylene stretched near the polar thiol group of Langmuir monolayers of semifluorinated thiols containing 10 fluorinated carbons (Fig. 6a), were increased by increasing the number of CH_2 groups from 6 to 10 then 12 or by increasing the length of the fluorinated segments from 6 to 8 and 10 in the molecules with a fixed 12 CH_2 groups (Fig. 6b). Such behavior implied that the increment of either the hydrogenated or fluorinated chain length increases the disordering effects (called *gauche* defects), which agrees well with the previous results of self-assembled monolayers of partially fluorinated thiols on gold.[69] Moreover, the orientation of the CF_3 group on these Langmuir mono-

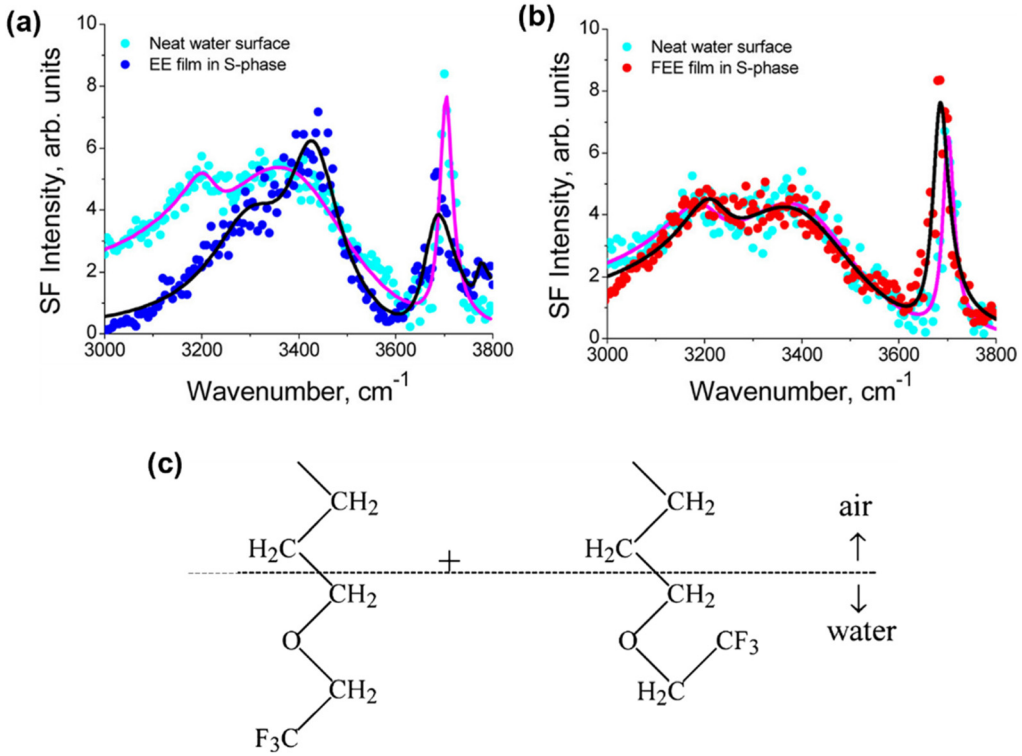

Fig. 5 SSP spectra of pure water surface (cyan circles) and (a) EE monolayer (blue circles) and (b) FEE monolayer (red circles). (c) Possible conformations of the FEE headgroup in the disordered monolayer-water transition zone. Reproduced from ref. 82 with permission from [American Chemical Society], copyright [2013].

Table 2 Assignments of CH stretches of Langmuir monolayers of alkanethiols, semifluorinated alkanethiols, alcohols, and carboxylic acids[77]

Normal modes of vibration	$H_{18}SH$	$F_{10}H_{10}SH$	$F_{10}H_{10}COOH$	$F_{10}H_{10}OH$
	Peak positions (±3 cm^{-1})			
CH_2-ss^G-symmetric stretch from *gauche* defects	2845	2845	2845	2845
CH_2-as^G-asymmetric stretch from *gauche* defects	2920	2920	2920	2920
CH_2-ss^P-symmetric stretch CH_2 near polar groups	n/a	2874	2868	2834
CH_2-as^P-asymmetric stretch CH_2 near polar groups	n/a	2944	2931	2890
CH_2-ss^F-symmetric stretch CH_2 near fluorinated groups	n/a	2881	2881	2881
CH_2-as^F-asymmetric stretch CH_2 near fluorinated groups	n/a	2938	2940	2941
CH_3-ss-symmetric stretch of methyl group	2883	n/a	n/a	n/a
CH_3-as-asymmetric stretch of methyl group	2965	n/a	n/a	n/a
CH_3-FR-Fermi Resonance of methyl group	2940	n/a	n/a	n/a

layers was also evaluated using the amplitude ratios of ssp/ppp and sps/ppp as well as the model calculations by Tyrode *et al.*[80] The SFG spectra of the **F10H10SH** Langmuir monolayer featured two prominent peaks at 1358 and 1378 cm^{-1} assigned to symmetric and asymmetric stretches of CF_3, respectively. The data also pointed out that the CF_3 groups in the Langmuir monolayers of **F10H6SH**, **F10H10SH**, **F10H12SH**, and **F8H12SH** have tilt angles ranging from 35° to 45° from the surface normal, exhibiting upright orientations of the fluorinated chains.

Thus, the studies have shown the versatility of SFG spectroscopy as one of the most useful techniques to investigate the structures at air–liquid interfaces due to its being highly surface specific. Especially, it can provide valuable information about the molecular orientations and conformations of fluorinated compounds on liquid–air surfaces. Although difficulties of SFG for studying liquid–air surfaces remain due to the lack of quantitative analyses, combining SFG with molecular dynamics calculations and/or other experimental techniques will stimulate further advances in the field in the future.

3. SFG spectroscopy to probe fluorinated material-based solid–air interfaces

Ji *et al.* pioneered the use of SFG spectroscopy to determine highly specific molecular-level information about the orien-

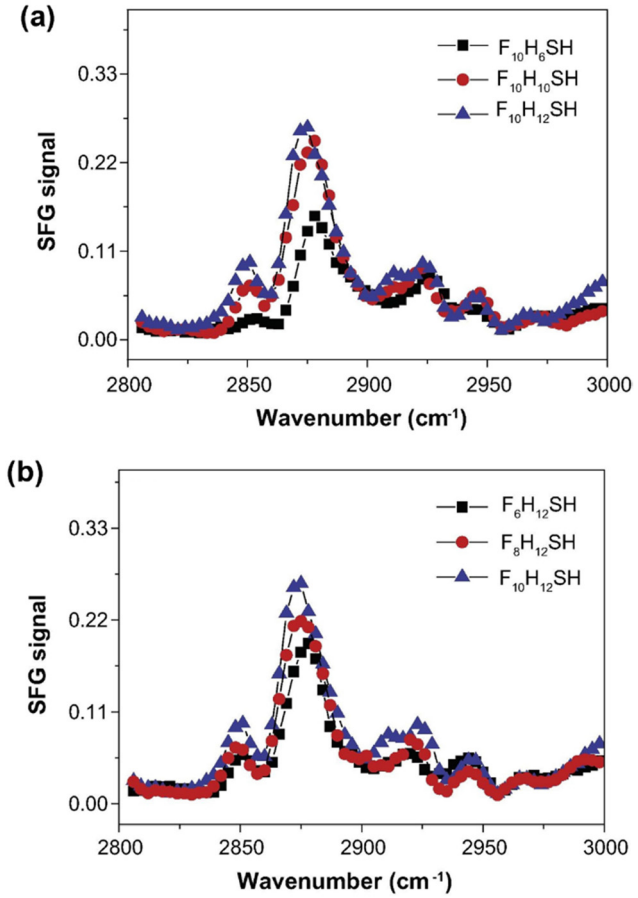

Fig. 6 SF spectra under ssp polarization combination of semifluorinated thiols possessing (a) the same number of the fluorinated segment with varying the length of the hydrogenated part and (b) the same number of the hydrogenated segment with varying the length of the fluorinated part. Reproduced from ref. 77 with permission from [Elsevier], copyright [2015].

tation of a fluorinated compound.[83] The authors use Teflon (poly(tetrafluoroethylene)) to generate thin films using shear-depositing techniques, as this technique forms highly oriented PTFE films.[84,85] Using this type of PTFE film is intended to settle the long-standing controversy surrounding the assignment of the CF_2 vibrational modes of PTFE. The study employed three distinct combinations of input and output polarizations: ssp, sps, and ppp (each letter denotes the type of polarization of SFG output, visible input, and infrared input, respectively). At 1142 cm^{-1} and 1204 cm^{-1}, the author claimed that only the sps polarization combination for the CF_2 band of the PTFE film was observed. To verify that the signal obtained originated from the PTFE/substrate, CCl_4 was added between the PTFE and the substrate. The absence of peaks from the CF_2 band of the PTFE film or CCl_4 indicated that CCl_4 must interfere with the ordered structure of the PTFE thin film. These results suggest that these two bands originate from the PTFE/substrate. To derive information from the SFG spectra, the author utilized existing vibrational mode studies of PTFE.[86] The author argued that, based on the helical structure of PTFE at room temperature, the normal vibration mode should have the following symmetries: A_1, A_2, E_1, or E_2. Nevertheless, infrared and Raman can only be activated in the E_1 symmetry mode. The author concluded, based on the observed sps polarization and E_1 mode, that the PTFE surface must be aligned along the shearing direction with the E_1 vibration mode. These studies represent the first utilization of SFG spectroscopy to identify the surface vibrational spectra of PTFE, which directly supports the assignment of the CF_2 vibrational modes of PTFE.

Later, Kristalyn and coworkers reported the use of SFG spectroscopy to study fluorinated materials at the solid–air interface.[87] The studies used fluoroalkylsilane adsorbate **FAS-17**, which is well-known for its high thermal stability, low surface energy, and exceptional hydrophobicity[88] to form organic thin films on SiO_2 substrates. The authors emphasized a key challenge of fluoroalkylsilane thin films is the formation of thin films that deviate from the ideal system (*e.g.*, heterogeneous multilayer thin films) *via* crosslinking of two- or three-dimensional structures due to the hydrolysis of the chlorosilane precursors to form bonds between adjacent molecules or between the silane absorbates and the substrates.[87,88] One of the factors affecting the homogeneity of silane adsorbates-based thin films is the fabrication variables such as deposition time, adsorbate concentration, and temperature.[88–90] Understanding how each factor affects the performance of developed thin films is critical for fluoroalkylsilane monolayers due to such thin films have been widely used to fabricate organic electronic devices.[91–94] Notably, these devices' performance and quality were dependent on the crystallinity and homogeneity of the silane thin films.[91–94] Thus, the authors reported the studies on the deposition of SAMs generated from the fluoroalkylsilane precursor **FAS-17** on SiO_2 over a time range of 2s to 5 and 20 minutes.

The resultant film's homogeneity was determined using SFG spectroscopy in conjunction with other surface techniques including ellipsometry and contact angle. SFG analysis revealed that the peak positions of both ssp and ppp polarizations were 1345 and 1370 cm^{-1} for fluorinated silane thin films generated after 5 and 20 minutes of developing time, respectively. These observed peaks have been attributed to the asymmetric CF_3 stretching. Interestingly, the two-second developing time resulted in the absence of the asymmetric CF_3 stretching peak at 1345 and 1370 cm^{-1} in the obtained film. The absence of SFG signals indicated that the silane monolayer thin film had insufficient surface coverage and lacked a well-ordered orientation. This phenomenon was also observed in contact angle studies with a significantly lower average contact angle of 89° for the thin firm generated by the shortest deposition time (2 s) compared to samples fabricated with a medium (5 min) or a long (20 min) deposition time, which had 111° and 110° contact angles, respectively.

At first glance, SFG and contact angle data for the thin films generated using a medium (5 min) and a long (20 min) deposition time suggested that both films had similar coverage

and orientation properties. Nonetheless, the authors noted that the formation of an inhomogeneous multilayer organic thin film was observed at the longest deposition time (20 min) with the ellipsometry thickness of 3.10 nm, which was 2–3 times greater than the expected monolayer thin film of the C10 carbon chain (1.34–1.6 nm) while the thin film generated using a medium deposition time (5 min) exhibited the monolayer thickness values of 1.42 nm with a tilted angle of approximately 29° to the surface normal.[94] Thus, combining SFG spectroscopy with other surface-sensitive techniques revealed useful information for identifying the optimal conditions for generating/preparing high-quality homogeneous SAMs from silane precursors and avoiding the formation of low-coverage/highly-disordered or heterogeneous multilayer thin films based on the deposition time.

Moreover, SFG techniques were also used in conjunction with infrared and Raman spectroscopies to deduce the molecular arrangement of buried perfluorosulfonated ionomer (PFSI) films such as Nafion at the solid–air interface on a Pt substrate. Nafion materials, one of the most widely used perfluorosulfonic acids, are important for proton transports in polymer electrolyte fuel cells (PEFCs). Yagi and coworkers investigated the molecular structure of six different PFSI thin films with thicknesses of 1, 2, 5, 9, 26, and 33 nm formed at Nafion interfaces on Pt substrates, as shown in Fig. 7.[95]

The results showed that the peak positions/shapes and intensities of several bands in the SFG spectrum of the Nafion thin films were independent of film thickness in the range of 9 to 33 nm, as illustrated in Fig. 8a. Interestingly, when the band thicknesses were less than 6 nm, a significant decrease in band intensity was observed. However, the authors discovered that SFG techniques have a much higher sensitivity than Raman spectroscopy, which is only effective on Nafion film with a thickness of 33 nm. Additionally, the authors characterized all the films by attenuated total reflection infrared spectroscopy (ATR-IR). Interestingly, the ATR-IR spectra of these Nafion thin films on Pt substrates were shaped differently compared to the SFG and Raman spectra and had some vibrational bands overlapping (Fig. 8b). The authors asserted that the multiple band overlaps resulted in significant changes in band shapes and slightly different band frequencies. The study also showed detailed assignments of each spectrum's peak positions.[95]

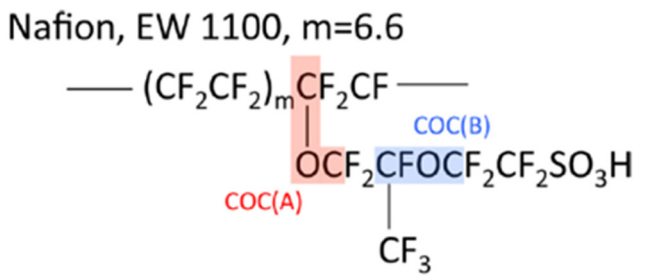

Fig. 7 Molecular structure of perfluorosulfonated ionomer (Nafion). Reproduced from ref. 95 with permission from [American Chemical Society], copyright [2014].

The authors primarily used the peak positions at ~1060 cm^{-1} of these spectra ($\nu_s(SO_3^-)$) to determine the molecular arrangement of the buried interfaces in these thin films. Plotting the IR intensities at ~1060 cm^{-1} for the Nafion films with different thicknesses revealed a linear correlation between the VSFG intensities at ~1060 cm^{-1} and the film thicknesses (Fig. 9, red squares). In comparison, the plot between the intensities of the SFG peaks and the film thicknesses showed an intensity saturation for the Nafion thin films with thickness greater than 6 nm (Fig. 9, blue circles). The authors explained the linear trend in the ATR-IR spectra by assuming that the ATR-IR technique detected all vibrational bands in Nafion thin films whereas SFG techniques detected signals only at the interface, where the thin film's inversion symmetry was broken. Thus, the increasing intensity trend of the ~1060 cm^{-1} SFG peak in the 1 to 5 nm films can be attributed to the single directionally ordered SO_3^- terminals at the interfaces while the plateau in signal intensity of this peak in the films with a thickness higher than 5 nm can be attributed to the SO_3^- terminal chain saturation toward the corresponding interfaces.

Based on this information, the authors proposed a molecular arrangement on the Nafion thin films with the SO_3^- terminal groups perpendicular to the interface to facilitate the signal acquisition, as shown in Fig. 10. The molecular arrangement depicted in Fig. 10a is less likely to be true because when the $\nu_s(SO_3^-)$ modes are oriented in opposite directions, the disappearance of the $\nu_s(SO_3^-)$ modes should be observed. Moreover, contact angle measurements with water on Nafion/Pt interfaces of 101.2° confirmed a hydrophobic interface nature, which is similar to the plasma-polymerized perfluorocarbon film.[96] Such hydrophobic surfaces are expected from the molecular arrangement depicted in Fig. 10b with the fluorinated side chains pointing to the interface rather than the arrangement depicted in Fig. 10c. Consequently, the author divided the molecular arrangement of PFSI molecules in the Nafion films formed on Pt surfaces into two regions based on these findings. The first region is within the 5 nm thickness and is purposed to align the PFSI molecules by orienting the hydrophobic part opposite to the Pt surface, as illustrated in Fig. 10b. In the second region, which appears in the films with thicknesses greater than 5 nm, the arrangement of sulfonate groups should maintain the inversion symmetry by establishing a random molecular arrangement to generate a macroscopic centrosymmetry.[97] As a result, the authors proposed that the molecular arrangement of PFSI molecules in Nafion films formed on surfaces of Pt combines the centrosymmetric and one-direction order of SO_3^- groups in two different regions, as illustrated in Fig. 11. Thus, this investigation showed that SFG techniques are crucial in determining thin film configurations that cannot be determined solely *via* the use of ATR-IR and/or Raman techniques.

In 2019, SFG spectroscopy was utilized by Okuno and colleagues to examine polymer thin films generated from two

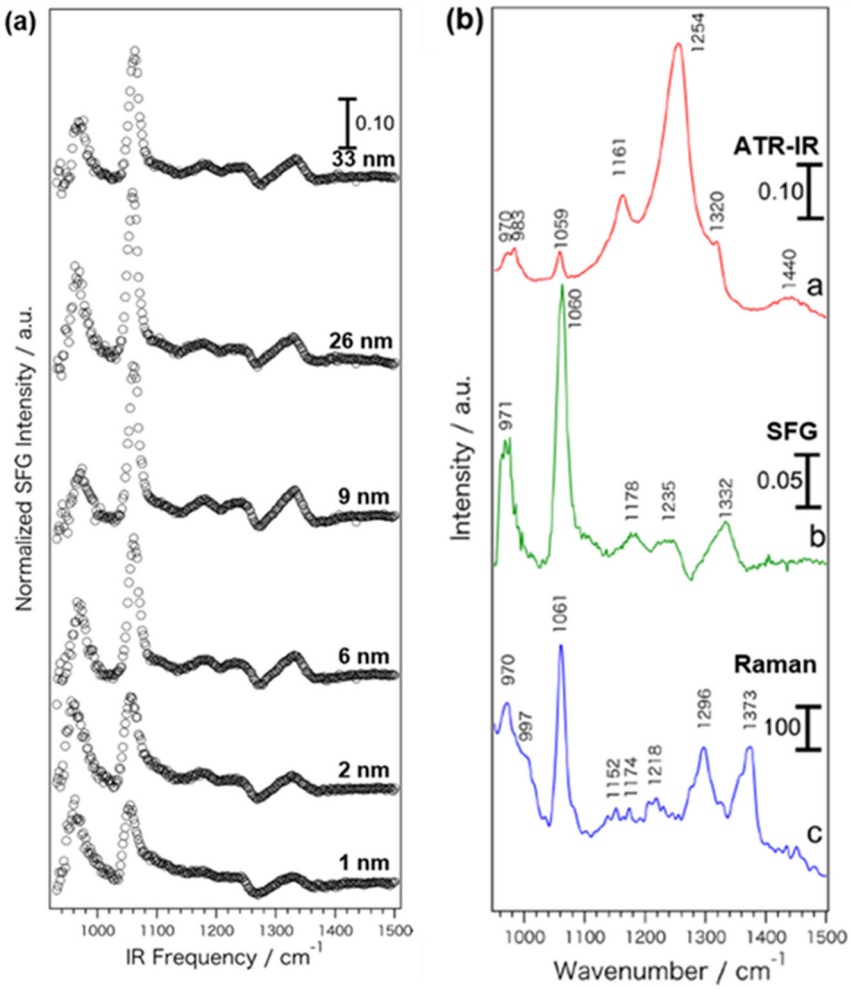

Fig. 8 (a) SFG spectra of Nafion thin films on Pt substrates with thicknesses of 1, 2, 6, 9, 26, and 33 nm. (b) ATR-IR, VSFG, and Raman spectra of Nafion thin film with 33 nm thickness. Reproduced from ref. 95 with permission from [American Chemical Society], copyright [2014].

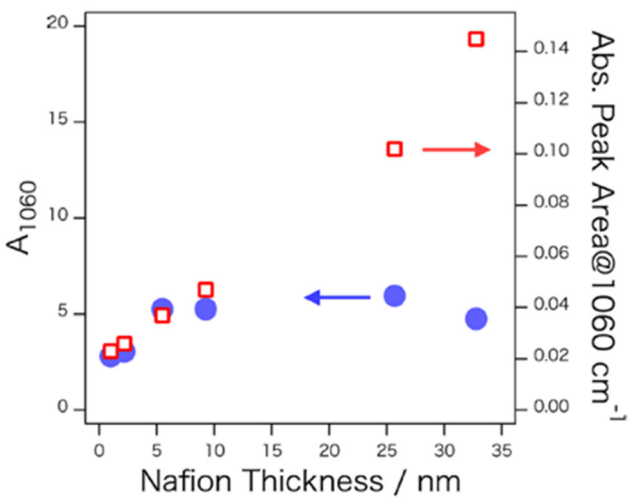

Fig. 9 Thickness depends on the integrated area of the IR absorption band and fitted amplitude A_{1060} and SFG band at ~1060 cm^{-1}. Reproduced from ref. 95 with permission from [American Chemical Society], copyright [2014].

different side chains of fluoroalkyl acrylate polymers: poly(2-perfluorohexylethyl acrylate) (p-C6FA) and poly(2-perfluoro-octylethyl acrylate) (p-C8FA).[98] The observation of such a large difference between the reported contact angles of p-C6FA and p-C8FA (47° and 110°, respectively) led to further orientation studies at the molecular level.[99] To confirm the molecular structure and conformation at the surface, the author used SFG spectroscopy in conjunction with other characterization techniques such as X-ray diffraction, Raman spectroscopy, and quantum chemical calculations. However, this review will focus only on the SFG studies.

According to previous research, the spectral band between 1300 and 1500 cm^{-1} can be used to determine the orientation of the terminal CF_3 group. To assign the band of the terminal CF_3 group within that range, the author used an air/PFNA solution as a reference, with the prepared PFNA solution concentration exceeding the critical micelle concentration since previous SFG reports on hydrogenated alkyl chains indicated that if the surfactant concentration was greater than the critical micelle concentration, the molecules of the surfactant will be

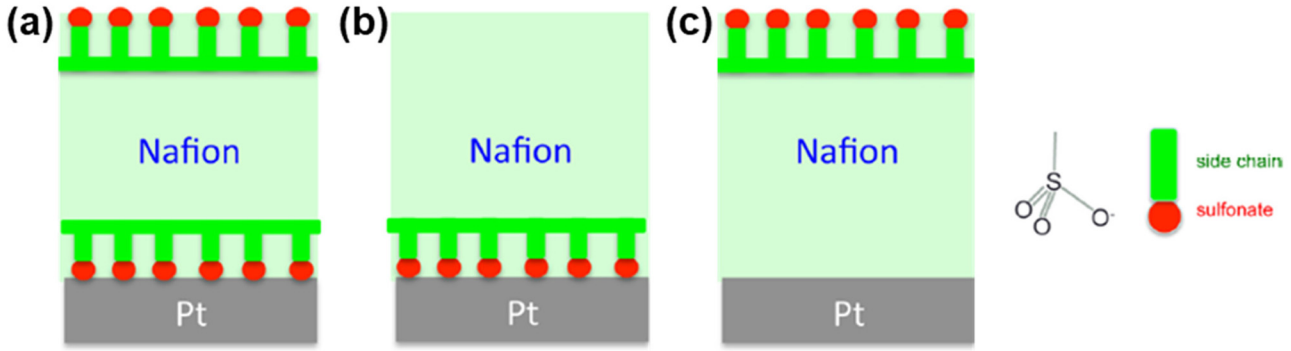

Fig. 10 Possible molecular arrangements of sulfonate terminals generated at (a) both Nafion–Pt and air–Nafion interfaces, (b) Nafion–Pt interface, and (c) air–Nafion interface. Reproduced from ref. 95 with permission from [American Chemical Society], copyright [2014].

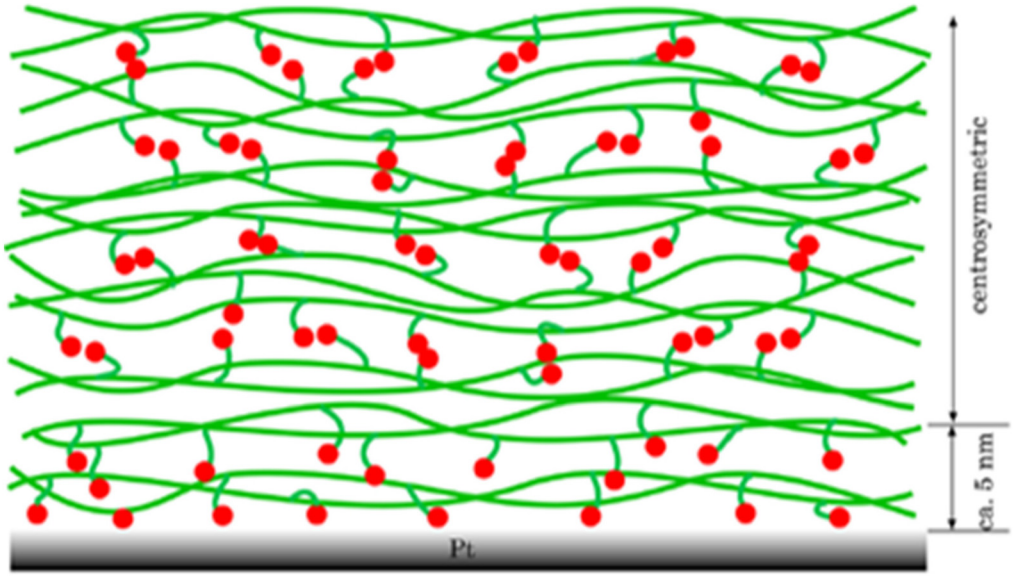

Fig. 11 Proposed molecular arrangement of PFSI molecules in Nafion films formed on Pt surfaces. Reproduced from ref. 95 with permission from [American Chemical Society], copyright [2014].

well-aligned.[100,101] Utilizing ssp, sps, and ppp polarization, the following results were obtained: both the major negative band and the major positive band at 1370 cm^{-1} were detected with ssp and ppp polarization, respectively. However, the vibration signature was not detected with the sps polarization combination. Based on all available data, the author concluded that the band at 1370 cm^{-1} belongs to the fluoroalkyl group, which is consistent with a previous study of the band at 1369 cm^{-1}, which belongs to the terminal CF_3 group.[80]

After determining which peak to examine, the authors continued their research using air/p-C6FA and air/p-C8FA interfaces. The results from the air/p-C8FA interface showed bands similar to the reference air/PFNA solution, with a negative band and a positive band at 1370 and 1377 cm^{-1} detected with ssp and ppp polarization, respectively, and no vibration signature from the sps polarization combination. No bands were observed in the ssp and sps polarizations at the air/p-C6FA interface, but a weak band was observed with the ppp polarization. Based on the SFG data, the author concluded that the p-C8FA interface was densely packed with the CF_3 terminal group pointing toward the air at an approximate tilt angle of <10°. Furthermore, the side chains of p-C6FA were oriented parallel to the interface and contained a number of *gauche* defects. This behavior was proposed by the author on the basis of dipole–dipole interactions, with the longer fluoroalkyl chains exhibiting stronger interactions and greater order in the film.[102] These results demonstrated that the band at 1370 cm^{-1} in SFG studies of fluorinated films can be used as a marker to detect the orientation of the CF_3 group and to predict the crystallinity of the film generated from a fluorinated compound.

In 2020, Marquez and coworkers reported the SFG studies of fluorinated organic thin films generated from fluorinated alkanethiols with a progressively increasing *n*-alkyl chain atop

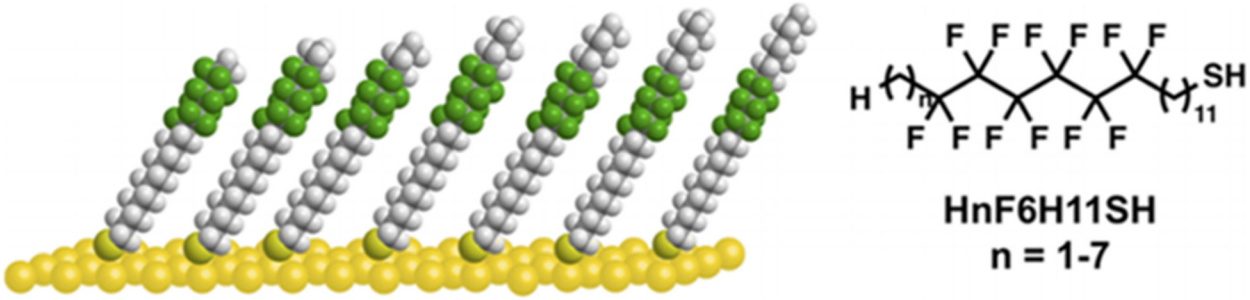

Fig. 12 Molecular structures of SAMs generated from the H*n*F6H11SH thiol series. Reproduced from ref. 4 with permission from [American Chemical Society], copyright [2020].

the fluorocarbon chain on Au substrates.[4] As illustrated in Fig. 12, the authors used a series of six fluorocarbon- and eleven hydrocarbon spacers equipped with seven different *n*-alkyl chain terminal groups (**H*n*F6H11SH**, where n = 1–7). These specific designs were chosen to capture the entire concept of the HC-FC inverted dipole and to fully comprehend its influence. The HC-FC inverted dipole is generated from methyl terminated fluorinated SAMs that exhibit an odd–even effect in unusual directions with an odd–even effect trend that is opposite to that of the CF_3-terminated thin films.[103] Several surface techniques were used to characterize the thin films in this study as well as their fully hydrocarbon counterparts including ellipsometry, XPS, PM-IRRAS, contact angle goniometry, and SFG. Interestingly, both contact angle goniometry and SFG studies revealed anomalous results.

The authors investigated contact angles with three distinct liquids: nonpolar liquids (decalin, hexadecane, bromonaphthalene, and perfluorodecalin), polar aprotic liquids (nitrobenzene, dimethylsulfoxide, dimethylformamide, and acetonitrile), and polar protic liquids (water, formamide, and glycerol). Unlike the contact angle data for fully hydrocarbon alkanethiol SAMs (**H*m*SH** with overall carbon count from 18 to 24), which showed that odd chains had lower contact angles than even chains in all types of liquid,[50,104] the contact angle trend for increasing the number of *n*-alkyl terminal chains atop a fluorocarbon chain (**H*n*F6H11SH**, total carbon count from 18 to 24) revealed strange patterns for all three types of liquids, as illustrated in Fig. 13. To better understand these unusual phenomena, the authors used SFG techniques to investigate the orientation of the terminal groups at the liquid–air interfaces on these fluorinated thin films. The antisymmetric ($\nu_{as}^{CH_3}$), symmetric ($\nu_{s}^{CH_3}$), and Fermi resonance ($\nu_{FR}^{CH_3}$) SFG peak positions of the terminal methyl C–H stretching on these film surfaces were indicated by gray dotted lines in Fig. 14 awhile the position of antisymmetric ($\nu_{as}^{CH_2}$) and symmetric methylene C–H stretching ($\nu_{s}^{CH_2}$) were indicated by black dotted lines in the same figure. Interestingly, drastically blue shifts were observed for the methyl C–H stretching $\nu_{as}^{CH_3}$ and $\nu_{s}^{CH_3}$ on shot terminal alkyl chain thin films (**H*n*F6H11SH**, where n = 1–3) compared to the SFG peak positions obtained from the films of longer terminal alkyl chains thiols (**H*n*F6H11SH**, where n = 4–7) and *n*-alkanethiol (**H18SH**). The authors hypothesized that the absence of blue shift for the longer terminal alkyl chain SAMs is due to the effect of the fluorinated carbons beneath the terminal alkyl chains dissipated after three CH_2 groups.

Further characterization of the SFG was carried out by examining the orientation of the terminal methyl group, particularly the tilt angle. The range of expected terminal methyl group tilt angles can be plotted using the SFG peak intensities of the antisymmetric $\nu_{as}^{CH_2}$ and symmetric $\nu_{s}^{CH_2}$ methylene C–H stretching peaks from ppp spectra, as shown in Fig. 14b. For nonpolar liquids such as decalin and hexadecane, the systematic decrease in contact angles for the **H*n*F6H11SH** SAMs with n = 1–3 can be explained by the unfavorable interactions between the underlying fluorinated moieties and the contact liquids, such unfavorable interactions decrease with the increase of the carbon number of the terminal alkyl chain. With the **H*n*F6H11SH** SAMs with n = 4–7, the dispersive effect was completely lost, with no detectable change in contact angle values. The same explanation also applies to the perfluorodecalin solvent with the favorable interaction between the liquid's fluorine moiety and the underlying fluorinated chains weakens when the length of alkyl chains increases, resulting in the rise of contact angle data and being consistent with the SFG data. Similarly, the increasing contact angle trends for polar aprotic solvents (DMSO, DMF, and ACN) and polar protic solvents (water, formamide, and glycerol) supported the hypothesis that the effect of the dipole–dipole interaction diminishes when the dipole becomes buried in the films. Additionally, the authors indicated that the odd–even effect was observed only on the **H*n*F6H11SH** SAMs with n = 1–7 when probing with nonpolar liquids due to the reported different tilt angles of the terminal methyl groups obtained from SFG data. The absence of an odd–even effect in polar aprotic and polar protic solvents is attributed to these liquids intercalating on the disordered top alkyl chains on the SAM surfaces. These findings have demonstrated that SFG techniques are critical and necessary tools for rationalizing the interfacial properties of fluorinated organic thin films. It is important to note, however, that the use of SFG data to interpret trends in contact angle date requires careful scrutiny

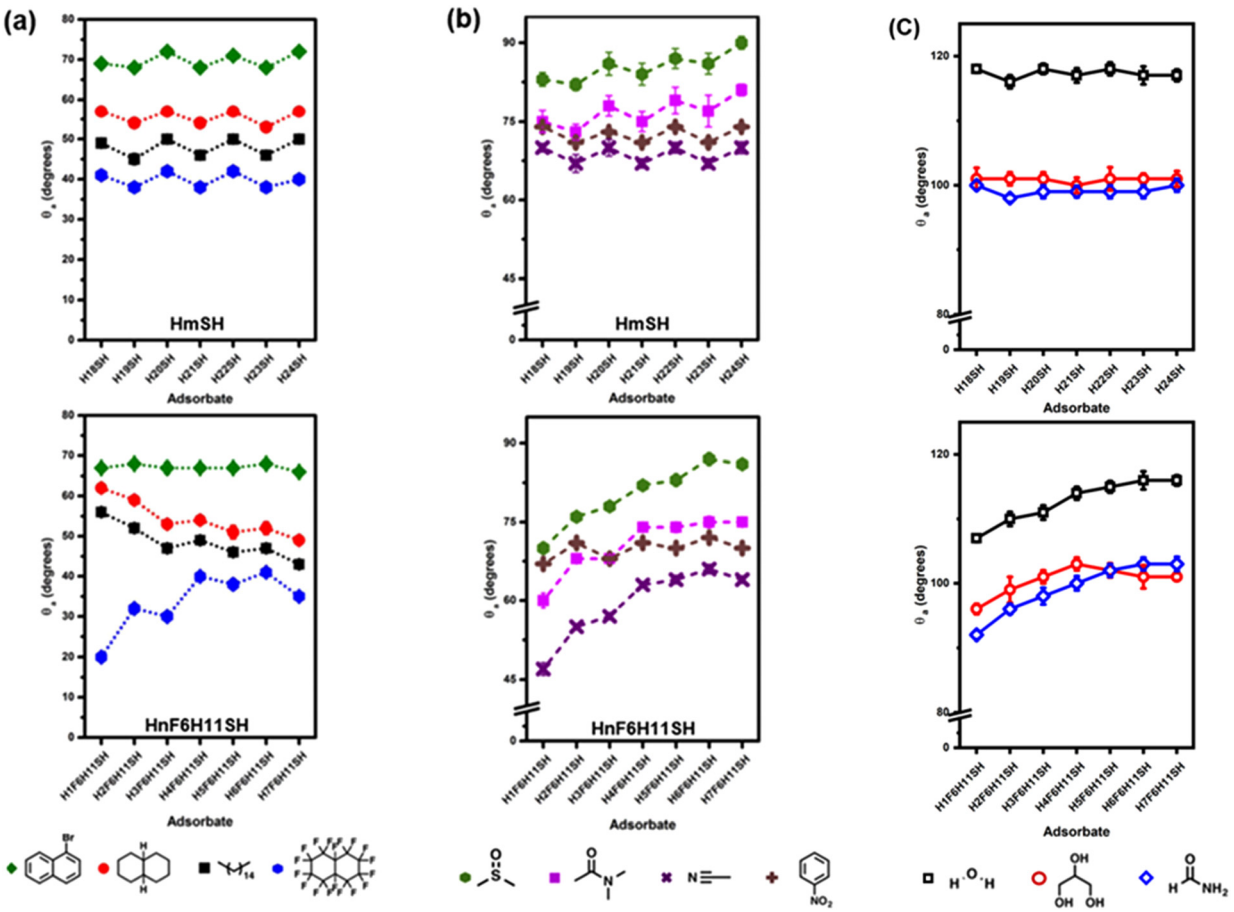

Fig. 13 Comparison of advancing contact angle values between H*m*SH and H*n*F6H11SH SAMs using different contacting liquids: (a) nonpolar liquids, (b) polar aprotic liquids, and (c) polar protic liquids. Reproduced from ref. 4 with permission from [American Chemical Society], copyright [2020].

because SFG spectra are carried out in air, and there is no liquid in contact with the molecular film.

Despite the fact that numerous studies on the orientation of fluorinated thin films on solid–air interfaces have been conducted, a straightforward explanation for the hydrophobic properties of fluorinated films with a strongly charged dipole moment at the interface has not been forthcoming. It is plausible, however, that strong dipole moments at the interface should interact strongly with highly polar liquids (*e.g.*, water) *via* charge–dipole or dipole–dipole interactions, leading to a high wettability of the polar liquid.[105,106] Nevertheless, the wettabilities of polar liquids on the Nafion/Pt fluorinated thin film appear hydrophobic in nature with a contact angle of 101.2° as previously mentioned.[95] This peculiar behavior prompted the hypothesis that a hydrophobic layer should exist on top of the fluorinated surface, which found experimental support in 2021 when Zhang and colleagues confirmed the existence of an ordered layer of hydrophobic-like water at a polytetrafluoroethylene (PTFE) interface.[107] The observed contact angle of 125° for water is consistent with hydrophobic behavior at the PTFE interface, which correlates with hydrophobic properties of the Nafion/Pt interface.[95]

In further studies, the observation of a water signal from SFG spectroscopy allowed for the examination of the hypothesized hydrophobic-like ordered water layer at the PTFE/Air interface. Three major SFG peaks at ~3280 cm^{-1}, ~3440 cm^{-1}, and 3680 cm^{-1} were used to validate the structure of the water layer. These peaks correspond to strongly H-bonded water molecules, loosely H-bonded water molecules, and the OH stretch of non-H-bonded water molecules (referred to as "dangling OH"), respectively. In addition, it was confirmed that the CaF_2/PTFE interface did not lead to the formation of a water layer by using D_2O as a test liquid. Testing the SFG signal from other substrates including PS/air, PET/air, and PVC/air surfaces also showed no sign of a water layer. These observations indicated that in the absence of the fluorinated moieties, which contain strong charged dipoles at the interface, no water layer is formed. To predict the orientation of the dangling OH, quantitative analysis of the SFG peak was fitted with the equation described in the literature. The authors concluded that both hydrogen-bonded and dangling OH groups were directed toward the PTFE film because all three bands displayed positive phase signs while the nonresonance was negative. This concept has been further supported by ultrafast vibrational dynamics techniques

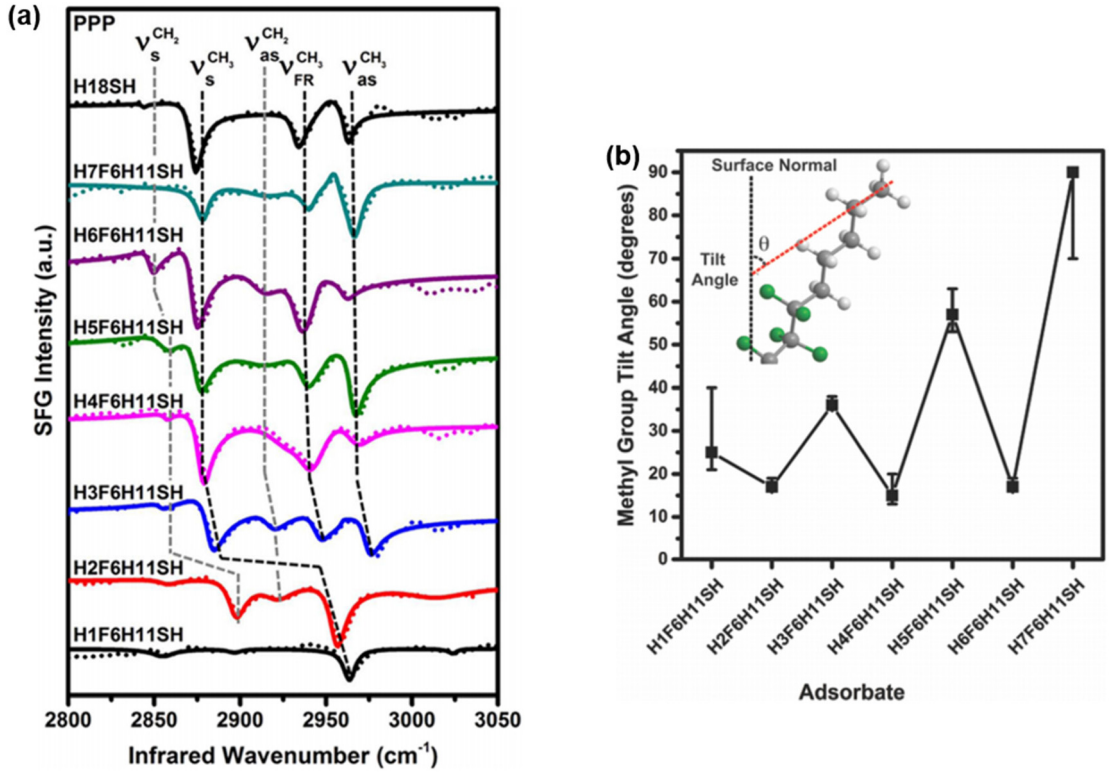

Fig. 14 Data obtained from H*n*F6H11SH fluorinated SAMs series. (a) Normalized SFG spectra for the C–H stretching region. The solid lines denote the fits to the spectra according to eqn (1). PPP denotes the polarization direction of the SFG, visible, and IR beams in that order with respect to the surface normal. The symmetric $\nu_s^{CH_3}$, and antisymmetric $\nu_{as}^{CH_3}$ methyl C–H stretching peak positions are marked with black dotted lines. (b) Average methyl group tilt angle of the H*n*F6H11SH fluorinated SAMs, derived from the SFG spectra. Reproduced from ref. 4 with permission from [American Chemical Society], copyright [2020].

that will not be discussed in this review because they fall outside of its scope. Similarly, the authors emphasized the previously reported behavior of OH pointing toward the interface of CCl_4/H_2O, which possesses a large charge–dipole interaction comparable to that of fluorinated moieties.[108]

Based on these findings, the authors concluded that the position of the dangling OH and the strength of the hydrogen bonds within the layer are responsible for the creation of an ordered water layer. This layer acts as a hydrophobic layer due to the confinement of a hydrogen-bond network at the macroscopic level on top of the hydrophilic nature at the molecular level of the PTFE film. With these considerations in mind, these SFG-based findings enable researchers to rationalize the surprising hydrophobic characteristics of dipole-containing fluorinated films in the presence of highly polar liquids.

4. SFG spectroscopy to probe fluorinated material-based solid–liquid interfaces

Despite the fact that several studies of the chemistry of fluorinated organic thin films have been reported and discussed in the previous sections, information regarding the interaction of contact liquids with thin film interfaces remained limited due to the scarcity of techniques available for detecting buried interfaces. Recently, Rodriguez and coworkers demonstrated the first study of surface dipoles causing uniform orientation of contacting polar liquids on CF_3 terminated thiol SAMs on gold using SFG techniques.[109] Specifically, the authors used SAMs derived from two partially fluorinated alkanethiols $CF_3(CH_2)_nSH$ (**F1H*n*SH** with n = 16 and 17), one partially deuterated fluorinated thiol $CD_3(CF_2)_6(CH_2)_{10}SH$ (**D1F6H10SH**), and a fully deuterated alkanethiol (**D18SH**, as a reference) to probe acetonitrile (CH_3CN), a polar aprotic solvent, with ppp and ssp SFG spectra. The SFG setup used in this study involved the interaction of a CaF_2 window and an Au substrate *via* the use of acetonitrile contact liquid. The authors began by examining the interaction between the CH_3CN/CaF_2 window and the CH_3CN/Au substrate separately in order to determine the signal contributions from these interfaces because the output signals from SFG technique can also interact with those layers, resulting in an additional signal toward the CH_3CN/SAM interface. The initial interaction study of the CH_3CN/CaF_2 window without a substrate revealed no signal in the ppp spectrum. The detected signal at 2245 cm^{-1}, which corresponds to nitrile stretching (CN stretching), was found to be tenfold lower than

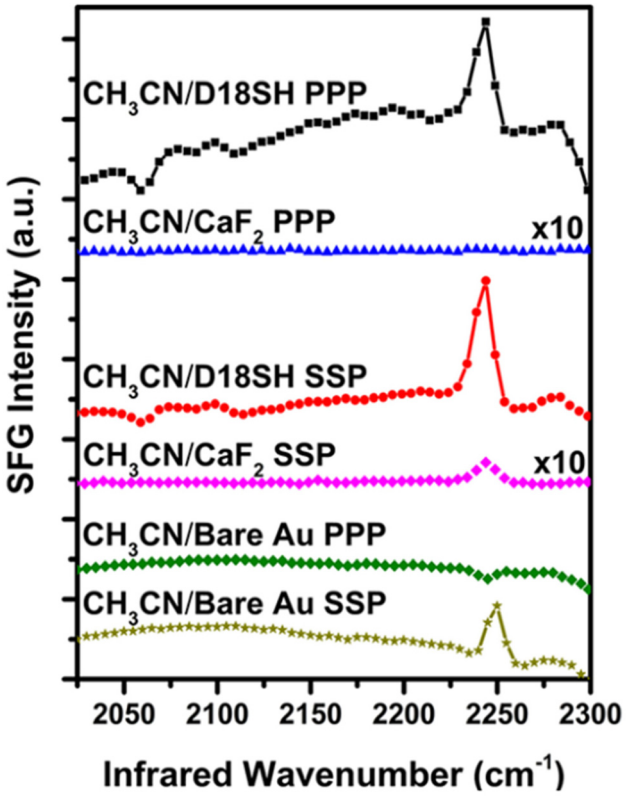

Fig. 15 SFG spectra in CN stretching region on different solid–liquid interfaces. Reproduced from ref. 109 with permission from [American Chemical Society], copyright [2020].

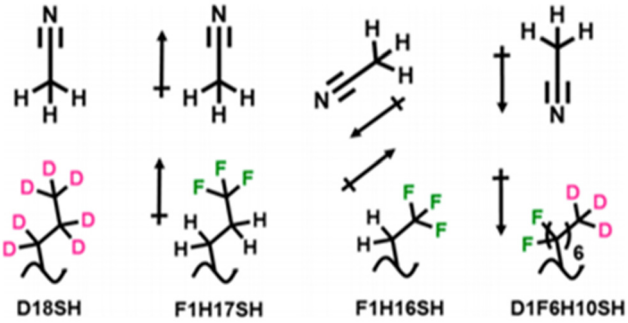

Fig. 16 Illustration of the hypothesis of acetonitrile orientations toward terminal fluorinated groups on SAMs. Reproduced from ref. 109 with permission from [American Chemical Society], copyright [2020].

the CN stretching signal obtained from the reference interface CH_3CN/D18SH, as shown in Fig. 15. According to the authors, the results signal from the CH_3CN/CaF_2 window had no effect on the CH_3CN/SAM interface. In comparison, the second CH_3CN/Au substrate interaction exhibited a distinct dip signal on ppp CN stretching and an asymmetric line shape on ssp CN stretching at 2245 cm^{-1}. However, the authors explained that these signals are associated with acetonitrile's preferential binding to Au, which is beyond the scope of this study because acetonitrile's preferential binding to Au should be mediated by an organic monolayer. Thus, no contribution effect of the CH_3CN/Au substrate on the CH_3CN/SAM interaction was observed.

Once the authors had established that no other interactions are interfering with the CH_3CN/SAM, the investigations were continued with solid–liquid interface studies of CH_3CN/SAM by using SFG spectra to determine the orientation of acetonitrile molecules in contact with SAMs derived from **F1H*n*SH** with n = 16 and 17, and **D1F6H10SH**. The authors identified the acetonitrile orientation based on the tilt of the terminal dipole moment in each developing thin film. Specifically, the fully trans-extended conformational order of **F1H17SH** molecules on their SAM made the terminal fluorinated group parallel to the surface normal, which should align the dipole moment position of acetonitrile in the same direction as the dipole moment generated by the terminal CF_3 group, head-to-tail (Fig. 16). Because **F1H16SH** contains one fewer carbon atom than **F1H17SH**, the tilt of the terminal CF_3 group for **F1H16SH** SAM is angled away from the surface normal. This allows a dipole moment to align differently from acetonitrile compared to the head-to-tail alignment from **F1H17SH**. Similar behavior was observed with **D1F6H10SH** thin film since it has the same overall carbon as **F1H16SH**. An illustration of this hypothesis is shown in Fig. 16.

These hypotheses have been confirmed by the results of SFG studies. Specifically, the ssp and ppp spectra observed from **D18SH** SAM served as internal references for interpreting the directional peaks, the peaks exhibited "dips" at 2060 and 2109 cm^{-1}, which correspond to the CD_3 group. The authors asserted that the dip characteristics are due to the CD_3 groups pointing away from the surface. Thus, "peak" can be interpreted in the opposite direction of "dips" (*i.e.*, toward the surface) as illustrated in Fig. 17a. Other interpretations of the "dips" and "peaks" in the CN and C–H stretching regions for ppp and ssp polarization combinations of acetonitrile in contact with **F1H*n*SH** (n = 16 and 17) and **D1F6H10SH** SAMs are shown in Fig. 17 along with a comparison of the expected peak orientations and the observed peak orientations obtained from SFG spectra (Table 3).[109]

Based on this information, the authors concluded that the methyl group of acetonitrile interacted with the **F1H17SH** SAM interface in a head-to-tail configuration, pointing toward the SAM surface (Fig. 16). The C–H SFG spectrum of the **F1H16SH** SAM exhibited a distinct dip, confirming that acetonitrile's CH_3 group points away from the surface. The CN spectrum of CH_3CN/**F1H16SH** surface exhibited an asymmetric peak with a negative amplitude. This indicated that the acetonitrile nitrile group points toward the **F1H16SH** SAM surface, possibly with antiparallel-oriented dipoles. Only dips in the SFG spectrum were observed at the CH_3CN/**D1F6H10SH** interface, indicating that the CH_3 moiety of the acetonitrile liquid is pointing away from the **D1F6H10SH** SAM surface and the CN group is pointing toward the surface of this thin film. This study showed that SFG techniques have a significant impact on investigating solid–liquid interfaces allowing to predict the orientation of

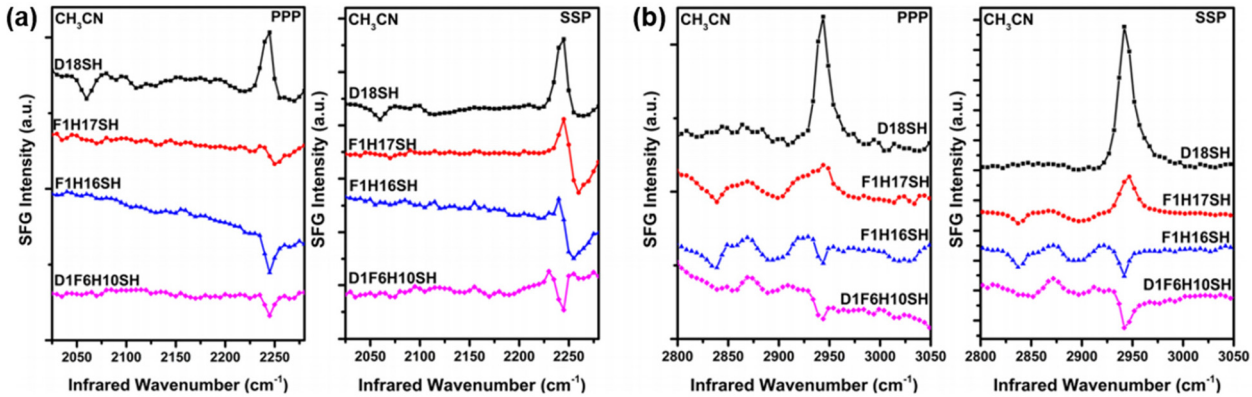

Fig. 17 SFG spectra on regions (a) CN stretching and (b) CH stretching from the CH_3CN/sample surfaces (CaF_2 window or bare gold). Reproduced from ref. 109 with permission from [American Chemical Society], copyright [2020].

Table 3 Comparison of expected and observed resonance orientations of acetonitrile liquid regarding acetonitrile methyl and nitrile stretching modes

		$\nu_{55}^{CH_3}$ resonance orientation		ν_{55}^{CN} resonance orientation	
Surface	Expected peak orientation[a]	Observed, ppp	Observed, ssp	Observed, ppp	Observed, ssp
Bare Au	↓	↑	↑	↓	↑
D18SH	↑	↑	↑	↑	↑
F1H17SH	↑	↑	↑	↓	↑
F1H16SH	↓	↓	↓	↓	↓
D1F6H10SH	↓	↓	↓	↓	↓

[a] The expected SFG resonance orientations are for both the CH_3 and CN modes and are based on intuition regarding van der Waals forces and permanent dipole-induced dipole interactions that can plausibly influence the acetonitrile-surface interactions.

the contact liquid toward underlying interfaces with different directions of dipole moment, thereby paving the way for one of the first direct evidence of the dipole-influenced wettability behavior of these unique model fluorinated surfaces.

5. Conclusions

This review article manifests the advantage of utilizing sum frequency generation vibrational spectroscopy (SFG-VS) techniques for the investigation of fluorinated material-based interfaces for further understanding of these liquid–air, solid–air, and solid–liquid interfaces. Specifically, SFG-VS methods provided valuable information about the orientations of fluorinated molecules at air–liquid interfaces, where the structure of an interface can be easily perturbed by changes at the surface. The polarization dependence of CF_3 and/or CF_2 stretch modes can be used to determine the orientation of monolayers at air–liquid interfaces. In addition, uncommon behaviors of the contacting liquids interacting with the monolayer thin films of fluorinated adsorbates, in which fluorinated groups act as a surrogate surface, can now be fully explained. Furthermore, with the dips and peaks characteristics obtained from SFG spectra at studied interfaces, the prediction of complex behaviors regarding contact liquid orientation toward the interfaces, which cannot be achieved with other surface techniques (*e.g.*, ellipsometry, contact angle goniometry, Raman spectroscopy, X-ray photoelectron spectroscopy, and infrared spectroscopy), can be interpreted. Based on these benefits of SFG-VS techniques, a more sophisticated understanding of the interfacial properties of monolayers can be achieved, which will bring positive impacts on the development of surface material sciences and their practical applications in the future.

Conflicts of interest

The authors declare no competing financial interest in this paper.

Acknowledgements

The authors are grateful for financial support from the National Science Foundation (CHE-2109174), the Robert A. Welch Foundation (Grant No. E-1320), and the Texas Center for Superconductivity at the University of Houston.

References

1 S. Lee, J.-S. Park and T. R. Lee, The wettability of fluoropolymer surfaces: influence of surface dipoles, *Langmuir*, 2008, **24**, 4817–4826.
2 E. Dhanumalayan and G. M. Joshi, Performance properties and applications of polytetrafluoroethylene (PTFE)—a review, *Adv. Compos. Hybrid Mater.*, 2018, **1**, 247–268.
3 I. S. Bayer, Superhydrophobic Coatings from Ecofriendly Materials and Processes: A Review, *Adv. Mater. Interfaces*, 2020, **7**, 2000095.

4 M. D. Marquez, O. Zenasni, D. Rodriguez, T. Yu, S. Sakunkaewkasem, F. T. Figueira, A. Czader, S. Baldelli and T. R. Lee, Burying the inverted surface dipole: Self-assembled monolayers derived from alkyl-terminated partially fluorinated alkanethiols, *Chem. Mater.*, 2020, **32**, 953–968.
5 S. Sakunkaewkasem, M. D. Marquez, H. J. Lee and T. R. Lee, Mixed phase-incompatible monolayers: Toward nanoscale anti-adhesive coatings, *ACS Appl. Nano Mater.*, 2020, **3**, 4091–4101.
6 C. de Alwis, T. R. Leftwich and K. A. Perrine, New Approach to Simultaneous In Situ Measurements of the Air/Liquid/Solid Interface Using PM-IRRAS, *Langmuir*, 2020, **36**, 3404–3414.
7 L. A. Alexandrova, L. S. Grigorov, N. A. Grozev and S. I. Karakashev, Investigation of Interfacial Free Energy of Three-Phase Contact on a Glass Sphere in Case of Cationic-Anionic Surfactant Aqueous Mixtures, *Coatings*, 2020, **10**, 573.
8 F. Zaera, Probing liquid/solid interfaces at the molecular level, *Chem. Rev.*, 2012, **112**, 2920–2986.
9 S. Sakunkaewkasem, M. A. Gonzalez, M. D. Marquez and T. R. Lee, Olefin-bridged bidentate adsorbates for generating self-assembled monolayers on gold, *Langmuir*, 2020, **36**, 10699–10707.
10 R. Atkin, S. Z. El Abedin, R. Hayes, L. H. S. Gasparotto, N. Borisenko and F. Endres, AFM and STM studies on the surface interaction of [BMP]TFSA and [EMIm]TFSA ionic liquids with Au(111), *J. Phys. Chem. C*, 2009, **113**, 13266–13272.
11 Y. Hu, D. Vanderah, G. Liu, W. Price, M. Mrksich and G. Scoles, A Comparative AFM Study of the Compressibility and Friction of Unmodified and Oligo (ethylene oxide)-Modified Alkane Thiol SAMs on Au(111) Using Nanografting, **https://www.nist.gov/publications/comparative-afm-study-compressibility-and-friction-unmodified-and-oligoethylene-oxide**.
12 G. Krämer and R. Bennewitz, Molecular Rheology of a Nanometer-Confined Ionic Liquid, *J. Phys. Chem. C*, 2019, **123**, 28284–28290.
13 M. Himmelhaus, F. Eisert, M. Buck and M. Grunze, Self-assembly of n-alkanethiol monolayers. A study by IR–Visible sum frequency spectroscopy (SFG), *J. Phys. Chem. B*, 2000, **104**, 576–584.
14 H.-F. Wang, L. Velarde, W. Gan and L. Fu, Quantitative sum-frequency generation vibrational spectroscopy of molecular surfaces and interfaces: lineshape, polarization, and orientation, *Annu. Rev. Phys. Chem.*, 2015, **66**, 189–216.
15 H.-F. Wang, W. Gan, R. Lu, Y. Rao and B.-H. Wu, Quantitative spectral and orientational analysis in surface sum frequency generation vibrational spectroscopy (SFG-VS), *Int. Rev. Phys. Chem.*, 2005, **24**, 191–256.
16 C. Hirose, N. Akamatsu and K. Domen, Formulas for the analysis of surface sum–frequency generation spectrum by CH stretching modes of methyl and methylene groups, *J. Chem. Phys.*, 1992, **96**, 997–1004.
17 C. Hirose, H. Yamamoto, N. Akamatsu and K. Domen, Orientation analysis by simulation of vibrational sum frequency generation spectrum: CH stretching bands of the methyl group, *J. Phys. Chem.*, 1993, **97**, 10064–10069.
18 S. A. Shah and S. Baldelli, Chemical Imaging of Surfaces with Sum Frequency Generation Vibrational Spectroscopy, *Acc. Chem. Res.*, 2020, **53**, 1139–1150.
19 W. Gan, D. Wu, Z. Zhang, R. Feng and H. Wang, Polarization and experimental configuration analyses of sum frequency generation vibrational spectra, structure, and orientational motion of the air/water interface, *J. Chem. Phys.*, 2006, **124**, 114705.
20 Y. R. Shen, Surface properties probed by second-harmonic and sum-frequency generation, *Nature*, 1989, **337**, 519–525.
21 S. Biswas, J. Kim, X. Zhang and G. D. Scholes, Coherent Two-Dimensional and Broadband Electronic Spectroscopies, *Chem. Rev.*, 2022, **122**, 4257–4321.
22 D. C. Duffy, P. B. Davies, C. D. Bain, R. N. Ward and A. M. Creeth, Sum-frequency Vibrational Spectroscopy of the Solid-Liquid Interface, *SPIE*, 1995, 2547.
23 J. D. C. Jacob, S. Rittikulsittichai, T. R. Lee and S. Baldelli, Characterization of SAMs derived from octadecyloxyphenylethanethiols by sum frequency generation, *J. Phys. Chem. C*, 2013, **117**, 9355–9365.
24 J. C. Love, L. A. Estroff, J. K. Kriebel, R. G. Nuzzo and G. M. Whitesides, Self-assembled monolayers of thiolates on metals as a form of nanotechnology, *Chem. Rev.*, 2005, **105**, 1103–1169.
25 T. Osaka, Creation of highly functional thin films using electrochemical nanotechnology, *Chem. Rec.*, 2004, **4**, 346–362.
26 C. Vericat, M. E. Vela, G. Benitez, P. Carro and R. C. Salvarezza, Self-assembled monolayers of thiols and dithiols on gold: new challenges for a well-known system, *Chem. Soc. Rev.*, 2010, **39**, 1805–1834.
27 X. Qiu, V. Ivasyshyn, L. Qiu, M. Enache, J. Dong, S. Rousseva, G. Portale, M. Stöhr, J. C. Hummelen and R. C. Chiechi, Thiol-free self-assembled oligoethylene glycols enable robust air-stable molecular electronics, *Nat. Mater.*, 2020, **19**, 330–337.
28 S. Casalini, C. A. Bortolotti, F. Leonardi and F. Biscarini, Self-assembled monolayers in organic electronics, *Chem. Soc. Rev.*, 2017, **46**, 40–71.
29 C. A. Smith, M. R. Narouz, P. A. Lummis, I. Singh, A. Nazemi, C.-H. Li and C. M. Crudden, N-Heterocyclic Carbenes in Materials Chemistry, *Chem. Rev.*, 2019, **119**, 4986–5056.
30 M. D. Porter, T. B. Bright, D. L. Allara and C. E. D. Chidsey, Spontaneously organized molecular assemblies. 4. Structural characterization of n-alkyl thiol monolayers on gold by optical ellipsometry, infrared spectroscopy, and electrochemistry, *J. Am. Chem. Soc.*, 1987, **109**, 3559–3568.
31 R. Colorado and T. R. Lee, Wettabilities of self-assembled monolayers on gold generated from progressively fluorinated alkanethiols, *Langmuir*, 2003, **19**, 3288–3296.

32 C. M. Wolff, L. Canil, C. Rehermann, N. N. Linh, F. Zu, M. Ralaiarisoa, P. Caprioglio, L. Fiedler, M. Stolterfoht, S. Kogikoski, I. Bald, N. Koch, E. L. Unger, T. Dittrich, A. Abate and D. Neher, Perfluorinated Self-Assembled Monolayers Enhance the Stability and Efficiency of Inverted Perovskite Solar Cells, *ACS Nano*, 2020, **14**, 1445–1456.

33 A. Hasan, S. K. Pattanayek and L. M. Pandey, Effect of Functional Groups of Self-Assembled Monolayers on Protein Adsorption and Initial Cell Adhesion, *ACS Biomater. Sci. Eng.*, 2018, **4**, 3224–3233.

34 A. C. Jamison, P. Chinwangso and T. R. Lee, in *Functional Polymer Films*, Wiley-VCH Verlag GmbH & Co. KGaA, Weinheim, Germany, 2011, pp. 151–217.

35 S. Krishnan, C. J. Weinman and C. K. Ober, Advances in polymers for anti-biofouling surfaces, *J. Mater. Chem.*, 2008, **18**, 3405.

36 Y. Li, M. Giesbers, M. Gerth and H. Zuilhof, Generic top-functionalization of patterned antifouling zwitterionic polymers on indium tin oxide, *Langmuir*, 2012, **28**, 12509–12517.

37 L. R. St. Hill, J. W. Craft, P. Chinwangso, H.-V. Tran, M. D. Marquez and T. R. Lee, Antifouling Coatings Generated from Unsymmetrical Partially Fluorinated Spiroalkanedithiols, *ACS Appl. Bio Mater.*, 2021, **4**, 1563–1572.

38 L. R. St. Hill, H.-V. Tran, P. Chinwangso, H. J. Lee, M. D. Marquez, J. W. Craft and T. R. Lee, Antifouling Studies of Unsymmetrical Oligo(ethylene glycol) Spiroalkanedithiol Self-Assembled Monolayers, *Micro*, 2021, **1**, 151–163.

39 U. Srinivasan, M. R. Houston, R. T. Howe and R. Maboudian, Alkyltrichlorosilane-based self-assembled monolayer films for stiction reduction in silicon micromachines, *J. Microelectromech. Syst.*, 1998, **7**, 252–260.

40 V. Akulova, A. Salamianski, I. Chishankov and V. Agabekov, Formation and tribological properties of octacosanoic acid monomolecular Langmuir–Blodgett films, *Soft Mater.*, 2022, **20**, 161–167.

41 J. Yang, M. Zhou, J. Liu, H. Wang and C. Weng, Fabrication and tribological properties of self-assembled monolayers of alkanethiols on nickel substrates, *Appl. Surf. Sci.*, 2021, **559**, 149963.

42 P. E. Laibinis and G. M. Whitesides, Self-assembled monolayers of n-alkanethiolates on copper are barrier films that protect the metal against oxidation by air, *J. Am. Chem. Soc.*, 1992, **114**, 9022–9028.

43 T. Patois, A. Et Taouil, F. Lallemand, L. Carpentier, X. Roizard, J.-Y. Hihn, V. Bondeau-Patissier and Z. Mekhalif, Microtribological and corrosion behaviors of 1H,1H,2H,2H-perfluorodecanethiol self-assembled films on copper surfaces, *Surf. Coat. Technol.*, 2010, **205**, 2511–2517.

44 S. Hu, Z. Chen and X. Guo, Inhibition Effect of Three-Dimensional (3D) Nanostructures on the Corrosion Resistance of 1-Dodecanethiol Self-Assembled Monolayer on Copper in NaCl Solution, *Materials*, 2018, **11**, 1225.

45 R. Zhao, W. Xu, Q. Yu and L. Niu, Synergistic effect of SAMs of S-containing amino acids and surfactant on corrosion inhibition of 316L stainless steel in 0.5 M NaCl solution, *J. Mol. Liq.*, 2020, **318**, 114322.

46 Y. Qiang, S. Fu, S. Zhang, S. Chen and X. Zou, Designing and fabricating of single and double alkyl-chain indazole derivatives self-assembled monolayer for corrosion inhibition of copper, *Corros. Sci.*, 2018, **140**, 111–121.

47 H. Mehta, G. Kaur, G. R. Chaudhary, N. Prabhakar, S. Kaul and N. K. Singhal, Evaluation of corrosion resistant, antimicrobial and cytocompatible behaviour of cobalt based metallosurfactants self-assembled monolayers on 316L stainless steel surface, *Surf. Coat. Technol.*, 2022, **444**, 128657.

48 H. Sellers, A. Ulman, Y. Shnidman and J. E. Eilers, Structure and binding of alkanethiolates on gold and silver surfaces: implications for self-assembled monolayers, *J. Am. Chem. Soc.*, 1993, **115**, 9389–9401.

49 A. Ulman, J. E. Eilers and N. Tillman, Packing and molecular orientation of alkanethiol monolayers on gold surfaces, *Langmuir*, 1989, **5**, 1147–1152.

50 R. G. Nuzzo, L. H. Dubois and D. L. Allara, Fundamental studies of microscopic wetting on organic surfaces. 1. Formation and structural characterization of a self-consistent series of polyfunctional organic monolayers, *J. Am. Chem. Soc.*, 1990, **112**, 558–569.

51 S. Bhattacharya, M. P. Yothers, L. Huang and L. A. Bumm, Interaction of the $(2\sqrt{3} \times 3)$rect. Adsorption-Site Basis and Alkyl-Chain Close Packing in Alkanethiol Self-Assembled Monolayers on Au(111): A Molecular Dynamics Study of Alkyl-Chain Conformation., *ACS Omega*, 2020, **5**, 13802–13812.

52 C. D. Bain, E. B. Troughton, Y. T. Tao, J. Evall, G. M. Whitesides and R. G. Nuzzo, Formation of monolayer films by the spontaneous assembly of organic thiols from solution onto gold, *J. Am. Chem. Soc.*, 1989, **111**, 321–335.

53 S.-C. Chang, I. Chao and Y.-T. Tao, Structure of self-assembled monolayers of aromatic-derivatized thiols on evaporated gold and silver surfaces: Implication on packing mechanism, *J. Am. Chem. Soc.*, 1994, **116**, 6792–6805.

54 R. Colorado Jr. and T. R. Lee, Physical organic probes of interfacial wettability reveal the importance of surface dipole effects, *J. Phys. Org. Chem.*, 2000, **13**, 796–807.

55 C. Du, Z. Wang, J. Chen, A. Martin, D. Raturi and M. Thuo, Role of Nanoscale Roughness and Polarity in Odd–Even Effect of Self-Assembled Monolayers, *Angew. Chem., Int. Ed.*, 2022, **61**, e202205251.

56 S. Carlson, M. Becker, F. N. Brünig, K. Ataka, R. Cruz, L. Yu, P. Tang, M. Kanduč, R. Haag, J. Heberle, H. Makki and R. R. Netz, Hydrophobicity of Self-Assembled Monolayers of Alkanes: Fluorination, Density, Roughness,

and Lennard-Jones Cutoffs, *Langmuir*, 2021, **37**, 13846–13858.

57 Y. Feng, E. R. Dionne, V. Toader, G. Beaudoin and A. Badia, Odd–Even Effects in Electroactive Self-Assembled Monolayers Investigated by Electrochemical Surface Plasmon Resonance and Impedance Spectroscopy, *J. Phys. Chem. C*, 2017, **121**, 24626–24640.

58 C. Du, R. S. Andino, M. C. Rotondaro, S. W. Devlin, S. Erramilli, L. D. Ziegler and M. M. Thuo, Substrate Roughness and Tilt Angle Dependence of Sum-Frequency Generation Odd–Even Effects in Self-Assembled Monolayers, *J. Phys. Chem. C*, 2022, **126**, 7294–7306.

59 F. B. Amara, E. R. Dionne, S. Kassir, C. Pellerin and A. Badia, Molecular Origin of the Odd–Even Effect of Macroscopic Properties of n-Alkanethiolate Self-Assembled Monolayers: Bulk or Interface?, *J. Am. Chem. Soc.*, 2020, **142**, 13051–13061.

60 C. D. Bain, J. Evall and G. M. Whitesides, Formation of monolayers by the coadsorption of thiols on gold: variation in the head group, tail group, and solvent, *J. Am. Chem. Soc.*, 1989, **111**, 7155–7164.

61 M. Graupe, M. Takenaga, T. Koini, R. Colorado and T. R. Lee, Oriented surface dipoles strongly influence interfacial wettabilities, *J. Am. Chem. Soc.*, 1999, **121**, 3222–3223.

62 C. E. D. Chidsey and D. N. Loiacono, Chemical functionality in self-assembled monolayers: structural and electrochemical properties, *Langmuir*, 1990, **6**, 682–691.

63 F. P. Zamborini and R. M. Crooks, Corrosion passivation of gold by n-alkanethiol self-assembled monolayers: Effect of chain length and end group, *Langmuir*, 1998, **14**, 3279–3286.

64 M.-W. Tsao, J. F. Rabolt, H. Schönherr and D. G. Castner, Semifluorinated/hydrogenated alkylthiol thin films: A comparison between disulfides and thiol binary mixtures, *Langmuir*, 2000, **16**, 1734–1743.

65 T. H. Ong, P. B. Davies and C. D. Bain, Sum-frequency spectroscopy of monolayers of alkoxy-terminated alkanethiols in contact with liquids, *Langmuir*, 1993, **9**, 1836–1845.

66 L. D. Ramos, S. de Beer, M. A. Hempenius and G. J. Vancso, Redox-induced backbiting of surface-tethered alkylsulfonate amphiphiles: Reversible switching of surface wettability and adherence, *Langmuir*, 2015, **31**, 6343–6350.

67 I. Wenzl, C. M. Yam, D. Barriet and T. R. Lee, Structure and wettability of methoxy-terminated self-assembled monolayers on gold, *Langmuir*, 2003, **19**, 10217–10224.

68 S. Patwardhan, D. H. Cao, G. C. Schatz and A. B. F. Martinson, Atomic Layer Deposition Nucleation on Isolated Self-Assembled Monolayer Functional Groups: A Combined DFT and Experimental Study, *ACS Appl. Energy Mater.*, 2019, **2**, 4618–4628.

69 O. Zenasni, A. C. Jamison and T. R. Lee, The impact of fluorination on the structure and properties of self-assembled monolayer films, *Soft Matter*, 2013, **9**, 6356–6370.

70 L. Hunter, A. M. Z. Slawin, P. Kirsch and D. O'Hagan, Synthesis and conformation of multi-vicinal fluoroalkane diastereoisomers, *Angew. Chem., Int. Ed.*, 2007, **46**, 7887–7890.

71 H. J. Lee, A. C. Jamison and T. R. Lee, Surface Dipoles: A Growing Body of Evidence Supports Their Impact and Importance, *Acc. Chem. Res.*, 2015, **48**, 3007–3015.

72 J. G. Petrov, T. D. Andreeva and H. Möhwald, Fluorination of the Hydrophilic Head Accelerates the Collapse of the Monolayer but Stabilizes the Bilayer of a Long-Chain Trifluoroethyl Ether on Water, *Langmuir*, 2006, **22**, 4136–4143.

73 M. Pabon and J. M. Corpart, Fluorinated surfactants: synthesis, properties, effluent treatment, *J. Fluorine Chem.*, 2002, **114**, 149–156.

74 J. G. Riess, Fluorous micro- and nanophases with a biomedical perspective, *Tetrahedron*, 2002, **58**, 4113–4131.

75 G. L. Gaines, Surface activity of semifluorinated alkanes: F(CF2)m(CH2)nH, *Langmuir*, 1991, **7**, 3054–3056.

76 Z. Huang, A. A. Acero, N. Lei, S. A. Rice, Z. Zhang and M. L. Schlossman, Structural studies of semifluorinated hydrocarbon monolayers at the air/water interface, *J. Chem. Soc., Faraday Trans.*, 1996, **92**, 545–552.

77 D. Volpati, A. Chachaj-Brekiesz, A. L. Souza, C. V. Rimoli, P. B. Miranda, O. N. Oliveira and P. Dynarowicz-Łątka, Semifluorinated thiols in Langmuir monolayers – A study by nonlinear and linear vibrational spectroscopies, *J. Colloid Interface Sci.*, 2015, **460**, 290–302.

78 P. B. Miranda and Y. R. Shen, Liquid Interfaces: A Study by Sum-Frequency Vibrational Spectroscopy, *J. Phys. Chem. B*, 1999, **103**, 3292–3307.

79 M. Bonn, Y. Nagata and E. H. G. Backus, Molecular Structure and Dynamics of Water at the Water–Air Interface Studied with Surface-Specific Vibrational Spectroscopy, *Angew. Chem., Int. Ed.*, 2015, **54**, 5560–5576.

80 E. Tyrode, C. M. Johnson, M. W. Rutland, J. P. R. Day and C. D. Bain, A Study of the Adsorption of Ammonium Perfluorononanoate at the Air–Liquid Interface by Vibrational Sum-Frequency Spectroscopy, *J. Phys. Chem. C*, 2007, **111**, 316–329.

81 T. Iwahashi, T. Miyamae, K. Kanai, K. Seki, D. Kim and Y. Ouchi, Anion configuration at the air/liquid interface of ionic liquid [bmim]OTf studied by sum-frequency generation spectroscopy, *J. Phys. Chem. B*, 2008, **112**, 11936–11941.

82 P. Karageorgiev, J. G. Petrov, H. Motschmann and H. Moehwald, Why fluorination of the polar heads reverses the positive sign of the dipole potential of Langmuir monolayers: a vibrational sum frequency spectroscopic study, *Langmuir*, 2013, **29**, 4726–4736.

83 N. Ji, V. Ostroverkhov, F. Lagugné-Labarthet and Y.-R. Shen, Surface Vibrational Spectroscopy on Shear-

Aligned Poly(tetrafluoroethylene) Films, *J. Am. Chem. Soc.*, 2003, **125**, 14218–14219.

84 H. Suzuki, K. Oiwa, A. Yamada, H. Sakakibara, H. Nakayama and S. Mashiko, Linear Arrangement of Motor Protein on a Mechanically Deposited Fluoropolymer Thin Film, *Jpn. J. Appl. Phys.*, 1995, **34**, 3937.

85 J. C. Wittmann and P. Smith, Highly oriented thin films of poly(tetrafluoroethylene) as a substrate for oriented growth of materials, *Nature*, 1991, **352**, 414–417.

86 B. P. Grady and S. L. Cooper, *The vibrational spectroscopy of polymers*, ed. D. I. Bower and W. F. Maddams, Cambridge University Press, New York, 1989, 326 pp. Price: $89.50, *J. Polym. Sci. Part C Polym. Lett.*, 1990, vol. 28, pp. 386–387.

87 C. B. Kristalyn, S. Watt, S. A. Spanninga, R. A. Barnard, K. Nguyen and Z. Chen, Investigation of sub-monolayer, monolayer, and multilayer self-assembled semifluorinated alkylsilane films, *J. Colloid Interface Sci.*, 2011, **353**, 322–330.

88 S. Onclin, B. J. Ravoo and D. N. Reinhoudt, Engineering silicon oxide surfaces using self-assembled monolayers, *Angew. Chem., Int. Ed.*, 2005, **44**, 6282–6304.

89 J.-M. Ducéré, A. Estève, A. Dkhissi, M. D. Rouhani and G. Landa, Evidence of self-assembled monolayers preorganization prior to surface contact: A first principles study, *J. Phys. Chem. C*, 2009, **113**, 15652–15657.

90 K. Wen, R. Maoz, H. Cohen, J. Sagiv, A. Gibaud, A. Desert and B. M. Ocko, Postassembly chemical modification of a highly ordered organosilane multilayer: new insights into the structure, bonding, and dynamics of self-assembling silane monolayers, *ACS Nano*, 2008, **2**, 579–599.

91 J. Rhee and H. H. Lee, Patterning organic light-emitting diodes by cathode transfer, *Appl. Phys. Lett.*, 2002, **81**, 4165–4167.

92 K. P. Pernstich, C. Goldmann, C. Krellner, D. Oberhoff, D. J. Gundlach and B. Batlogg, Shifted transfer characteristics of organic thin film and single crystal FETs, *Synth. Met.*, 2004, **146**, 325–328.

93 K. P. Pernstich, S. Haas, D. Oberhoff, C. Goldmann, D. J. Gundlach, B. Batlogg, A. N. Rashid and G. Schitter, Threshold voltage shift in organic field effect transistors by dipole monolayers on the gate insulator, *J. Appl. Phys.*, 2004, **96**, 6431–6438.

94 C. Huang, H. E. Katz and J. E. West, Solution-processed organic field-effect transistors and unipolar inverters using self-assembled interface dipoles on gate dielectrics, *Langmuir*, 2007, **23**, 13223–13231.

95 I. Yagi, K. Inokuma, K. Kimijima and H. Notsu, Molecular structure of buried perfluorosulfonated ionomer/pt interface probed by vibrational sum frequency generation spectroscopy, *J. Phys. Chem. C*, 2014, **118**, 26182–26190.

96 Y. Zhang, G. H. Yang, E. T. Kang, K. G. Neoh, W. Huang, A. C. H. Huan and D. M. Y. Lai, Characterization of fluoropolymer films deposited by magnetron sputtering of poly (tetrafluoroethylene) and plasma polymerization of heptadecafluoro-1-decene (HDFD) on (100)-oriented single-crystal silicon substrates, *Surf. Interface Anal.*, 2002, **34**, 10–18.

97 D. K. Paul, K. Karan, A. Docoslis, J. B. Giorgi and J. Pearce, Characteristics of self-assembled ultrathin nafion films, *Macromolecules*, 2013, **46**, 3461–3475.

98 M. Okuno, O. Homma, A.-T. Kuo, S. Urata, R. Koguchi, T. Miyajima and T. Ishibashi, Molecular Orientations and Conformations of Air/Fluoroalkyl Acrylate Polymer Interfaces Studied by Heterodyne-Detected Vibrational Sum Frequency Generation, *Macromolecules*, 2019, **52**, 8705–8712.

99 Y. Katano, H. Tomono and T. Nakajima, Surface Property of Polymer Films with Fluoroalkyl Side Chains, *Macromolecules*, 1994, **27**, 2342–2344.

100 D. E. Gragson, B. M. McCarty and G. L. Richmond, Ordering of Interfacial Water Molecules at the Charged Air/Water Interface Observed by Vibrational Sum Frequency Generation, *J. Am. Chem. Soc.*, 1997, **119**, 6144–6152.

101 J. C. Conboy, M. C. Messmer and G. L. Richmond, Investigation of Surfactant Conformation and Order at the Liquid–Liquid Interface by Total Internal Reflection Sum-Frequency Vibrational Spectroscopy, *J. Phys. Chem.*, 1996, **100**, 7617–7622.

102 T. Hasegawa, T. Shimoaka, N. Shioya, K. Morita, M. Sonoyama, T. Takagi and T. Kanamori, Stratified Dipole-Arrays Model Accounting for Bulk Properties Specific to Perfluoroalkyl Compounds, *ChemPlusChem*, 2014, **79**, 1421–1425.

103 O. Zenasni, M. D. Marquez, A. C. Jamison, H. J. Lee, A. Czader and T. R. Lee, Inverted surface dipoles in fluorinated self-assembled monolayers, *Chem. Mater.*, 2015, **27**, 7433–7446.

104 P. E. Laibinis, G. M. Whitesides, D. L. Allara, Y. T. Tao, A. N. Parikh and R. G. Nuzzo, Comparison of the structures and wetting properties of self-assembled monolayers of n-alkanethiols on the coinage metal surfaces, copper, silver, and gold, *J. Am. Chem. Soc.*, 1991, **113**, 7152–7167.

105 T. Hasegawa, Physicochemical Nature of Perfluoroalkyl Compounds Induced by Fluorine, *Chem. Rec.*, 2017, **17**, 903–917.

106 T. Shimoaka, Y. Tanaka, N. Shioya, K. Morita, M. Sonoyama, H. Amii, T. Takagi, T. Kanamori and T. Hasegawa, Surface properties of a single perfluoroalkyl group on water surfaces studied by surface potential measurements, *J. Colloid Interface Sci.*, 2016, **483**, 353–359.

107 J. Zhang, J. Tan, R. Pei, S. Ye and Y. Luo, Ordered Water Layer on the Macroscopically Hydrophobic Fluorinated Polymer Surface and Its Ultrafast Vibrational Dynamics, *J. Am. Chem. Soc.*, 2021, **143**, 13074–13081.

108 F. G. Moore and G. L. Richmond, Integration or Segregation: How Do Molecules Behave at Oil/Water Interfaces?, *Acc. Chem. Res.*, 2008, **41**, 739–748.

109 D. Rodriguez, M. D. Marquez, O. Zenasni, L. T. Han, S. Baldelli and T. R. Lee, Surface dipoles induce uniform orientation in contacting polar liquids, *Chem. Mater.*, 2020, **32**, 7832–7841.

